EXPERIMENTAL INVESTIGATION

OF NONLINEAR COUPLED VIBRATIONS

OF BARS AND PLATES

by

Bernd C. Schneider

B.A.Sc., University of British Columbia, 1967

A Thesis Submitted in Partial Fulfillment of the
Requirements for the Degree of
Master of Applied Science
In the Department
of
Mechanical Engineering

We accept this thesis as conforming to
the required standard

THE UNIVERSITY OF BRITISH COLUMBIA

April, 1969

In presenting this thesis in partial fulfilment of the requirements for an advanced degree at the University of British Columbia, I agree that the Library shall make it freely available for reference and Study. I further agree that permission for extensive copying of this thesis for scholarly purposes may be granted by the Head of my Department or by his representatives. It is understood that copying or publication of this thesis for financial gain shall not be allowed without my written permission.

Department of Mechanical Engineering

The University of British Columbia
Vancouver 8, Canada

Date April 30, 1969

TABLE OF CONTENTS

		Page
	ABSTRACT	i
	ACKNOWLEDGEMENT	iii
	LIST OF FIGURES	iv
	LIST OF TABLES	v
	LIST OF APPENDICES	vi
	NOMENCLATURE	vii
CHAPTER I	DEFINITION OF THE PROBLEM	1
	Introduction	1
	Statement of the Problem	3
	Literature Survey	3
	Limitations of the Study	4
	Definitions	5
CHAPTER II	THEORETICAL CONSIDERATIONS	6
	Derivation of the Differential Equations of Motion for a Beam Under Plane Motion	6
	Discussion of the Derived Equations	11
CHAPTER III	APPARATUS AND INSTRUMENTATION	14
	Signal Flow	14
	Individual Instruments	18
	Test Bed and Frame	21
	Suspension	22
	Plate Support	23
	Bar Clamp	23
	Models and Boundary Conditions	24
	Circular Plate	24
	Cantilever Bar	25
	Strain Gauges and Bridges	25
	Circular Plate	25
	Cantilever Bar	26
	Bridges	26

Page

CHAPTER IV TESTING..... 27

Calibration and Check Out..... 27
Test Procedure..... 28
Constant Power Plot Discussion..... 30
Interpretation of Frequency Spectra.. 33
Chladni Figures..... 34
Plotting and Photography..... 34

CHAPTER V EXPERIMENTAL RESULTS..... 35

Circular Plate..... 35
Cantilever Bar..... 37

CHAPTER VI DISCUSSION OF EXPERIMENTAL RESULTS..... 41

Circular Plate..... 41
Cantilever Bar..... 43

CHAPTER VII SUMMARY AND CONCLUSION..... 47

Suggestions for Future Research..... 47
Summary..... 48
Conclusion..... 50

BIBLIOGRAPHY..... 52

APPENDIX..... 53

ABSTRACT

The theory presented describes the physical phenomenon of nonlinear coupling of longitudinal and flexural vibrations when a beam is excited transversely at high frequencies. Equations are derived based on the Bernoulli-Euler theory of flexure, by energy methods, to describe the transverse and the longitudinal vibration of a beam of constant cross-section under plane motion. The initial crookedness of the beam and the longitudinal inertia, accounted for in the theory, give rise to the coupled vibrations. No closed form solution is presented. However, a simple analysis of some of the coupling terms suggests the existence of several coupled vibrations. By the method proposed herein, the frequencies of these vibrations can be established. In particular, the theory predicts two longitudinal coupled vibrations with the frequency ratio 1:2.

The agreement between the theory and the experimental results is good. The vibrations predicted exist and the frequency ratio for the predicted longitudinal vibrations was 1:2. Further, the experimental results indicate that there are more longitudinal vibrations than indicated by the theory. A longitudinal coupled vibration at three times the frequency of transverse excitation was recorded. There are indications in the data that coupled flexural vibrations at twice the frequency of transverse excitation exist.

A circular plate centrally supported and transversely excited was also tested. Two pronounced resonant radial vibrations were recorded. The frequency ratio was 1:2. Coupled flexural vibrations were not identified.

The influence of the longitudinal vibration on the flexural vibration of the beam is examined. The limitations of the theory, of the experiment, and the significance of the resonant strains is discussed.

ACKNOWLEDGEMENT

I wish to express my gratitude to my advisors, Dr. C.R. Hazell and Dr. H. Ramsey, for giving me the opportunity to work on this challenging project and for granting me so much latitude in my work.

Further, I take this opportunity to thank all the technicians and secretaries in the Department for contributing directly, or indirectly, to the research.

This study was made possible through research grant No. 9513-07 provided by the Defense Research Board of Canada.

LIST OF FIGURES

Figure		Page
1.	Extension and Rotation of Central Plane Fiber.....	7
2.	Reference Axis for Displacement Measurements.....	9
3.	Signal Flowchart.....	15
4.	Overall View of the Instrumentation.....	18
5.	Test Bed.....	21
6.	Bar Suspension.....	22
7.	Constant Acceleration and Approximated Constant Power Frequency Spectra.....	31
8.	Chladni Figures for the Transverse Vibration of the Circular Plate.....	35
9.	Chladni Figures for the Transverse Vibration of the Cantilever Bar.....	38
10.	Waveforms at Resonance for Circular Plate.....	39
11.	Waveforms at Resonance for Cantilever Bar.....	40
A-12.	Graphical Addition of Sinusoids Frequency Ratio 2....	54
A-13.	Graphical Addition of Sinusoids Frequency Ratio 3....	56
C-14.	Tangential Strain Frequency Spectra for Circular Plate.....	60
C-15.	Radial Strain Frequency Spectra for Circular Plate...	61
C-16.	Radial plus Bending Strain Frequency Spectra for Circular Plate.....	62
C-17.	Bending plus Axial Frequency Spectra for Cantilever Bar.....	63
C-18.	Axial Strain Frequency Spectra for Cantilever Bar....	64

LIST OF TABLES

		Page
Table 1	Allowable Acceleration Level.....	30
Table 2	Non-Dimensionalized Nodal Radii for Plate.....	36
Table 3	Non-Dimensionalized Nodal Distances for Bar.....	38
Table 4	Theoretical Resonant Frequencies for the Transverse Vibration of the Circular Plate.....	41
Table 5	Non-Dimensionalized Theoretical Nodal Distances for a Cantilever Beam.....	43
Table 6	Theoretical Resonant Frequencies for Flexural Vibrations of the Beam.....	44

LIST OF APPENDICES

		Page
APPENDIX A	Addition of Two Sinusoids.....	53
APPENDIX B	Linear Equations for Plate and Beam.....	57
APPENDIX C	Approximate Constant Power Frequency Spectra.....	60

NOMENCLATURE

Symbol

a	= diameter of plate, in
f	= frequency, cycles per second
g	= acceleration of gravity, in/sec^2
h	= bar and plate thickness, in
r	= radial distance, in
t	= time, sec
W	= deflection from static equilibrium position, in
$\overline{W}$	= static deflection of bar, or beam, in (includes deflection due to initial crookedness)
W_x, U_x	= partial derivative of a displacement with respect to the variable x
A	= cross-section of beam, in^2
D	= plate stiffness
E	= modulus of elasticity, lb/in^2
I	= moment of inertia
T	= period, sec
V	= volume, in^3
θ	= angle, radians
ν	= Poisson's ratio
φ	= mass/volume
ω	= frequency, radians per second
Δ	= increment of some variable

Abbreviations

BAM	= bridge amplifier and meter
CRO	= cathode ray oscilloscope
Hz	= cycles per second
RMS	= root-mean-square value of a function
J_o	= Bessel function of the first kind, integral order o
Y_o	= Bessel function of the second kind, integral order o
I_o	= Modified Bessel function of the first kind, integral order o
K_o	= Modified Bessel function of the second kind, integral order o

CHAPTER I

DEFINITION OF THE PROBLEM

Introduction

The application of the simple linear thin-plate theory at frequencies of order 10 KHz encountered in this experimental investigation is not appropriate. Additional phenomena arise in the mechanism of acoustic energy transmission under these circumstances to those encountered in the audible frequency range usually considered in architectural acoustics. An analysis by means of the simple linear theory indicates for the upper end of the acoustic frequency range that in plates the wavelengths of longitudinal and flexural waves are of the same order of magnitude; at frequencies much below the above frequency range the wavelength of the two types of waves differ by an order of magnitude. Consequently, there is the likelihood of coupling between the two types of waves at the upper end of the frequency range swept out in the experiment, whereas the coupling seems to be insignificant at frequencies much below 10 KHz.

A simple model was set up to explain the physical phenomenon of acoustic energy transmission at the upper frequency range encountered in the experiment. Following the approach taken by Mettler ($\bar{5}$)*, that is, energy methods and the Bernoulli-Euler theory of flexure, the coupled differential equations of motion for a beam of constant, prismatic cross section under plane motion were derived. The formulation of the problem differs from the usual linear theory essentially in one respect - the assumed strain expression. The equations account for the initial crookedness, or initial displacement, as

* barred numbers in parenthesis designate references in the Bibliography.

well as for an usually omitted inertia term. The initial crookedness and the longitudinal inertia term account for the coupled vibrations recorded in the experiment. The limitations of the two theories, the linear uncoupled theory and the non-linear coupled theory, are essentially the same, namely those of the Bernoulli-Euler theory of flexure. The bending strain is assumed to be directly proportional to the distance from the central plane. Plane cross sections are assumed to remain plane, that is, the shear deformation is ignored. Rotary inertia is omitted and damping is ignored. Summarizing, the proposed theory differs from the linear theory in that strains in the central plane are assumed to exist, whereas they are ignored in the linear theory.

No closed form solution is presented for the equations of motion derived. However, an examination of some of the second order coupling terms indicates the existence of coupled vibrations. Thus, for a beam excited at the supports, transversely, the analysis of the following terms, $\bar{W}_{xx}W_x$, $\bar{W}_xW_{xx}$, W_xW_{xx}, from the coupled equations indicates the existence of two longitudinal vibrations with the frequency ratio of 1:2. Using the fact that there are two coupled longitudinal vibrations, one can interpret the mixed second order coupling terms in the complimentary equation in the same manner. Effecting the necessary substitutions, two coupled transverse vibrations with the frequency ratio 1:2 should occur. These represent the influence of the longitudinal vibration on the transverse vibration. The method adopted in the interpretation indicates only the existence of the coupled vibration. It does not give any indication of their relative magnitude; it does not throw any light on the influence of the longitudinal vibration on the flexural vibration. Simply, the method just indicates the frequencies of the coupled vibrations.

Statement of the Problem

The purpose of this study was:

(1) to set up and check out the vibration system,

(2) to determine analytically and to interpret the coupled differential equations of motion for a beam of prismatic cross-section, under plane motion,

(3) to verify, experimentally, the occurrence of the coupled vibrations, in the longitudinal direction,

(4) to locate, experimentally, along the frequency spectrum line, where the predicted resonant vibrations occur,

(5) to determine the importance of the associated resonant vibrations, and

(6) to determine for a circular plate supported and excited transversely in the center the same experimental information as for the bar.

Literature Survey

To the best of the author's knowledge, the literature contains no record of the observance of acoustic coupling in bars, or plates. Theoretically, this coupled vibration has not been treated before. Up to the present time the transverse vibration of the bar, or the plate, has been treated dissociated from the longitudinal vibrations. Moreover, the longitudinal vibration has been considered without regard to the transverse vibrations.

The existence of strains in the central plane was postulated by mathematicians and stress analysts a long time ago. Pearson ($\bar{6}$) and ($\bar{7}$) showed that a beam under uniform transverse load does have strains in the

central plane; from physical considerations it is known that a non-developable surface has strains in the central plane. In the field of statics, Timoshenko (10) used this fact to derive the deflection for a circular plate. To the knowledge of the author strains in the central plane have not been previously considered for the dynamic case. Mettler (5) perhaps came closest to the solution for the case of a beam in plane motion. In his derivation, he retained the most significant terms of the strain expression, thereby obtaining coupling terms of the desired kind. There is no indication in his paper that he recognized the significance of these terms.

Limitations of the Study

The prime reason for undertaking this study was to verify experimentally the existence of the coupled vibrations in the plate and in the bar. The limitations of the experimental investigation are as follows. Because of the available system, the experiment was restricted to 'approximate constant power' frequency spectra. Since the strain level was very small, the desired signal often vanished in the electronic noise and induced electromagnetism. The experimental investigation was restricted to 10 KHz. The assumed boundary conditions could not be realized in practice for the cantilever bar. A solid plate could not be simulated. It was impossible to identify, independently from the spectral strain record, the nonlinear coupled flexural vibrations.

The analytical expressions derived have limitations too. First, the study is limited to nearly flat surfaces and those structures able to develop bending stresses; second, the derived equations are not exact - the limitations of the Bernoulli-Euler theory of flexure are present. The method adopted in interpreting the coupled differential equations indicates only the frequency of the coupled vibrations. The method adopted does not indicate

the absolute amplitudes involved.

Definitions

Approximated Constant Power Plot - the plotting procedure used in the spectral analysis. Briefly, it is the break-up of the frequency spectrum into short, constant acceleration segments making use of the maximum available power of the system. For a full discussion of this method, see section Constant Power Plot Discussion.

Node - a line, a point, or surface in a standing wave where some characteristic of the wave field has zero amplitude.

First Coupled Resonant Longitudinal (Radial) Vibration - longitudinal (radial) vibration at the same frequency as the excitation frequency in the transverse direction for the beam (plate).

Second Coupled Resonant Longitudinal (Radial) Vibration - longitudinal (radial) vibration at twice the frequency of the transverse vibration of the beam (plate). It occurs at half the frequency of the excitation as for the first longitudinal (radial) vibration.

Third Coupled Resonant Longitudinal Vibration - longitudinal vibration at thrice the frequency of the excitation in the transverse direction. It occurs at one third the frequency of the excitation for the first longitudinal vibration.

CHAPTER II

THEORETICAL CONSIDERATIONS

Derivation of the Differential Equations of Motion for a Beam Under Plane Motion

As the first step towards the deduction of the equations of motion for a beam under plane motion, the strain expression has been derived. For the development of the strain expression for strains in the neutral plane for an initially deflected line segment, a geometric approach is taken. Love ($\overline{3}$) presents a mathematical derivation. The difference between the equation deduced herein and the one in the above cited work lies in the fact that in the derivation presented an initial deflection curve is assumed and that the dynamic deflections are measured relative to it. Love's deduction assumes a fixed coordinate system in which the initial deflection of any point of the neutral plane is zero. The initial deflection curve assumed includes the static displacement of the beam from a perfectly flat surface and any effects due to the non-homogeneity of the material. Also, since the longitudinal inertia is an integral part in the proposed theory, the second order term W_x^2 has been retained in the strain expression. Since an elastic system is assumed, the Lagrangian definition of strain is used throughout.

The barred letters in Fig. 1 refer to the stationary system, that is, these coordinates account for the initial crookedness, static displacement, and any existing non-homogeneity. A fiber of the central plane is shown.

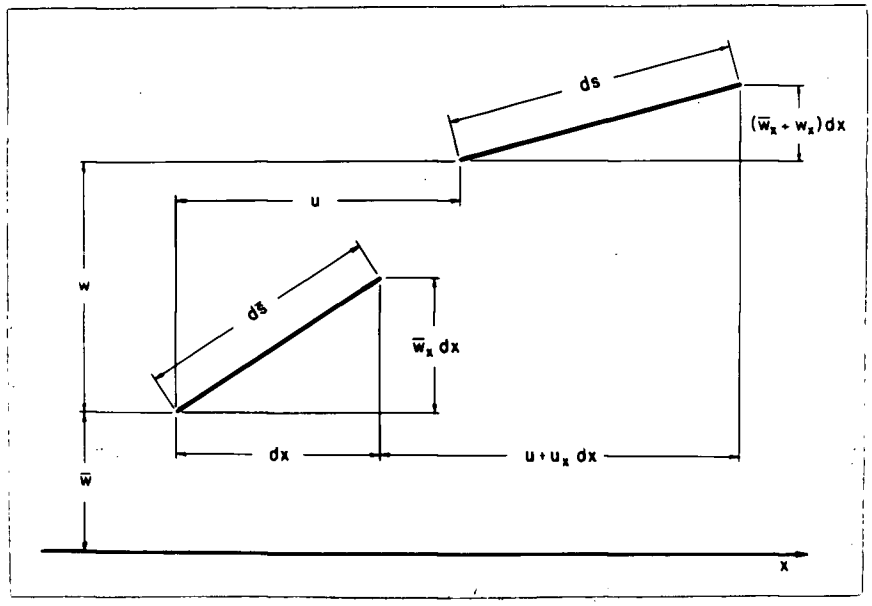

Fig. 1. Extension and Rotation of Central Plane Fiber

Before deformation, a line element of the axis of the beam has the length

$$d\bar{s} = (1 + \bar{W}_x^2)^{\frac{1}{2}} dx$$

when the beam has been deformed, the length is

$$ds = \left[(1 + U_x)^2 + (\bar{W}_x + W_x)^2 \right]^{\frac{1}{2}} dx$$

The elongation of the axis of the beam is given by

$$ds - d\bar{s} = \left[(1 + U_x)^2 + (\bar{W}_x + W_x)^2 \right]^{\frac{1}{2}} dx - (1 + \bar{W}_x^2)^{\frac{1}{2}} dx$$

Expanding each radical by the binomial theorem, keeping second order terms of the same type, the total strain becomes

$$\varepsilon_x = \frac{U_x + \bar{W}_x W_x + \frac{1}{2}(U_x^2 + W_x^2)}{1 + \frac{1}{2}\bar{W}_x^2}$$

Since small transverse initial displacements are considered, one is entitled

to write

$$\varepsilon_x = U_x + \bar{W}_x W_x + \frac{1}{2}(U_x^2 + W_x^2) \qquad (1)$$

This is the most general strain expression for the strains in the central plane of a beam for static, or dynamic deflections in two orthogonal directions.

The above expression is complete as it stands. However, an estimate based on the experimental findings indicated that the term U_x^2 is approximately two orders of magnitude smaller than W_x^2. For this reason, the term U_x^2 in the strain expression is omitted in further derivations.

The coupled equations of motion for the beam were derived by Mettler (5). In the derivation of the equations of motion, the basic assumptions of the Bernoulli-Euler theory of flexure are adopted. Accordingly, it is assumed that the bending strains vary linearly with the distance from the middle surface. Plane cross-sections are assumed to remain plane, that is, the shear deformation is neglected. Rotary inertia effects are ignored. Further, internal and external damping and distributed transverse loads are not considered.

Let $\bar{W}(x)$ be the initial deflection of the beam and $W(x,t)$ be the dynamic deflection of the beam measured relative to the initial deflection curve as shown in Fig. 2.

The first assumption made is that there are strains in the central plane of the beam. These can arise from the non-developability of the central surface, from distributed transverse loads, or from longitudinal inertia. How the resulting strain is made up, that is, whether strains induced by inertia effects predominate over strains due to the non-

developability of the surface, is not discussed in this thesis.

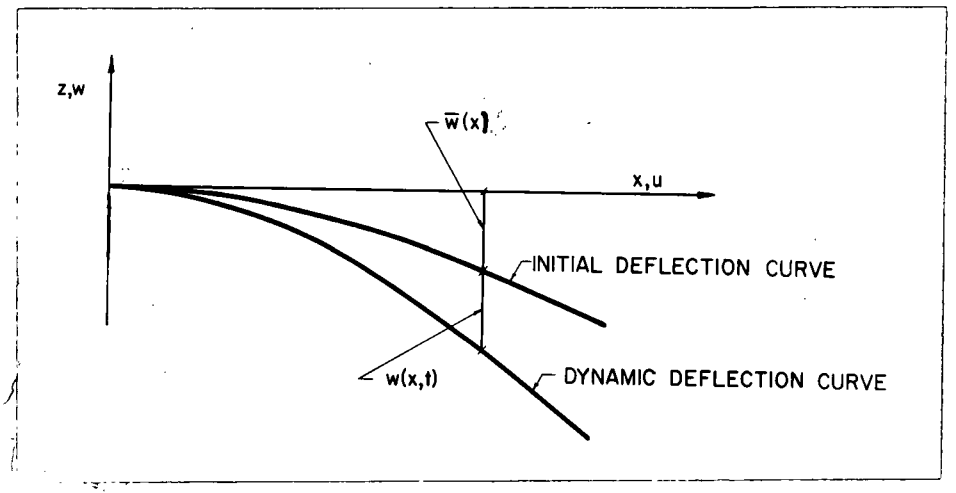

Fig. 2. Reference Axis for Displacement Measurements

The additional extension of a fiber at a distance z from the axis is

$$\varepsilon_1 = - z W_{xx}$$

This follows from the usual beam bending theory, or from the assumption that plane cross-sections do remain plane. The total strain is therefore,

$$\varepsilon = \varepsilon_x + \varepsilon_1$$

The next major assumption is, as is usually done in the beam bending theory, that stresses occur only in the x-direction. The elastic strain energy becomes

$$U = \frac{E}{2} \int_V \varepsilon^2 \, dV$$

and carrying out the partial integration over the cross section of a prismatic beam

$$U = \frac{EA}{2} \int_0^L (U_x + \bar{W}_x W_x + \frac{1}{2} W_x^2)^2 \, dx + \frac{EI}{2} \int_0^L W_{xx}^2 \, dx$$

The kinetic energy is given by

$$T = \frac{A\varphi}{2} \int_0^L (U_t^2 + W_t^2)\, dx$$

Making use of Hamilton's Principle

$$\delta \int_{t_1}^{t_2} (U - T)\, dt = 0 \tag{2}$$

Effecting the necessary substitutions, using Calculus of Variations, one obtains

$$- EA\, (U_x + \tfrac{1}{2} W_x^2 + W_x \bar{W}_x)_x + \varphi A\, U_{tt} = 0 \tag{3}$$

$$EIW_{xxxx} - EA \left[(U_x + \tfrac{1}{2} W_x^2 + W_x \bar{W}_x)\, (W_x + \bar{W}_x) \right]_x + \varphi A W_{tt} = 0 \tag{4}$$

These equations are the coupled nonlinear differential equations of motion for a beam under plane motion. These equations are based on the simplified strain expression. If the full strain expression is used, or if U_x is of the same order of magnitude as W_x, one obtains the following set of equations

$$- EA \left\{ \left[U_x + \bar{W}_x W_x + \tfrac{1}{2} (U_x^2 + W_x^2) \right] (1 + U_x) \right\}_x + \varphi A U_{tt} = 0 \tag{5}$$

$$EI\, W_{xxxx} - EA \left\{ \left[U_x + \bar{W}_x W_x + \tfrac{1}{2} (U_x^2 + W_x^2) \right] (\bar{W}_x + W_x) \right\}_x + \varphi A\, W_{tt} = 0 \tag{6}$$

The above equations, (5) and (6), differ from (3) and (4) respectively, only by the inclusion of the term U_x^2 in the strain expression. This term might be significant for explaining coupling frequencies higher than twice the frequency of the excitation, and it might become important for excitations

much higher than those used in this research.

To check the deduction, the equations are linearized

$$EA\, U_{xx} = A\, \varphi\, U_{tt} \quad \therefore \quad U_{xx} = \frac{1}{c^2}\, U_{tt} \tag{7}$$

and

$$EI\, W_{xxxx} + A\, \varphi\, W_{tt} = 0 \tag{8}$$

The first of these equations corresponds to the classical longitudinal vibration of rods; the second of these equations corresponds to the lateral vibration of a beam.

Discussion of the Derived Equations

In the paragraphs which follow the interpretation and the significance of particular coupling terms of the equations of motion for the beam are discussed. Even though the method assumed is qualitative in nature, some concrete predictions can be made.

We consider now the equation of motion (3) for the beam. Differentiating and rearranging the equation, one obtains

$$-U_{xx} + \frac{1}{c^2} U_{tt} = \bar{W}_{xx}\, W_x + \bar{W}_x\, W_{xx} + W_x\, W_{xx} \tag{9}$$

Assuming the flexural displacement to be of the form

$$W = F(x) \cos \omega t$$

so that

$$W_x\, W_{xx} = H(x) \cos^2 \omega t \tag{10}$$

and

$$\bar{W}_{xx}\, W_x = H_1(x) \cos \omega t \tag{11}$$

$$\bar{W}_x\, W_{xx} = H_2(x) \cos \omega t \tag{12}$$

where $\bar{W}_x$ and $\bar{W}_{xx}$ are just functions of x .

From analytical geometry

$$\cos^2 \omega t = \frac{1}{2}(1 + \cos 2\omega t)$$

therefore, $$W_x W_{xx} = H_3(x)\left[1 + \cos 2\omega t\right] \tag{13}$$

Next, it is assumed that the terms on the right-hand side of (9) are forcing functions. Substituting expressions (11), (12), and (13) for the terms on the right hand side of (9), one obtains

$$-U_{xx} + \frac{1}{c^2} U_{tt} = \left\{ H_1(x) + H_2(x) \right\} \cos \omega t + H_3(x) \left\{ 1 + \cos 2\omega t \right\} \tag{14}$$

By analogy, expanding, differentiating, and rearranging as was done above, one can write (4) in the following form,

$$EI\, W_{xxxx} - EA\left[U_{xx} W_x + U_x W_{xx} \right] + A\varphi W_{tt} = EA\left[U_{xx} \bar{W}_x + U_x \bar{W}_{xx} \right] \tag{15}$$

Having established, analytically and experimentally, the fact that there are at least two longitudinal coupled vibrations, one might substitute their expressions, guided by the approach taken for the longitudinal vibrations, for the right-hand side cross products of (15). As a consequence one should expect also two transverse, or flexural coupled vibrations, with the frequency ratio of 1:2. These would represent the influence of longitudinal vibrations on the transverse vibration.

In examining the expression (14) and (15) one can draw the following conclusion:

Expression (14):

At any one instant of time the longitudinal vibration of the beam is the result of two different, superimposed, sinusoidal excitations,

the frequencies of which are in the ratio of 1:2. Moreover, at least two different resonant frequencies are to be expected - one fundamental at the frequency of flexural vibration; the second at twice the frequency of transverse vibration.

Expression (15):

Making use of the fact that the beam is excited longitudinally by two forcing functions of frequency ω and 2ω, one can show that the right-hand side of (15) consists of the following functions

$$G_1(x) \cos \omega t + G_2 (x) \cos 2 \omega t$$

Two attendant resonant frequencies are to be expected.

CHAPTER III

APPARATUS AND INSTRUMENTATION

Signal Flow

The signal flowchart is shown in Fig. 3. Essentially, the instrumentation consisted of a vibration control feedback system and ancillary instruments to record diverse signals. Thus, a sound level meter was used for dynamic sound pressure waveform recording and frequency reference. The output was displayed either on the CRO, or on the level recorder. An optical non-contacting displacement transducer, called a Fotonic Sensor (MTI Instruments Division, Latham, N.Y.), was used as an independent frequency reference. The output was displayed on the CRO. Finally, a BAM and strain gauges were used for frequency spectra recording and waveform analysis.

The vibration control loop consisted of the generator, amplifiers, electromagnetic exciter, and accelerometer. The generator (henceforth called the control unit) sent out a pre-programmed signal, corresponding to the vibration level, to the 50 lbs. force vector exciter; the actual vibration level was sensed by the accelerometer mounted rigidly on the adapter for the specimen. The vibration level as recorded by the accelerometer was compared with the set point vibration level. Any error between the set point control and the feedback signal was corrected by the vibration control unit. For synchronization of the generator and the frequency calibrated paper on the level recorder an electrical connection was provided between these two units. Finally, a signal proportional to the acceleration

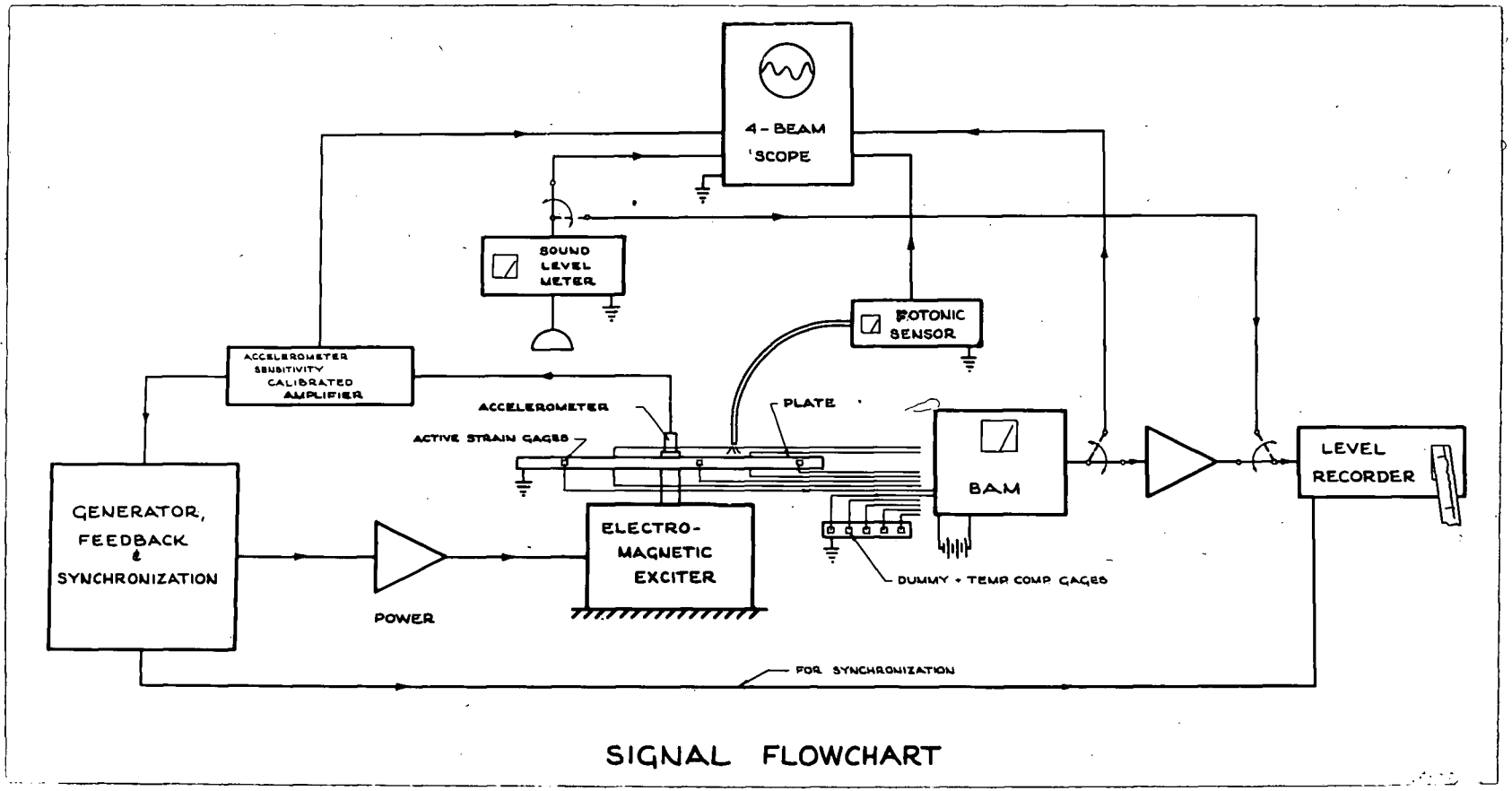

Fig. 3. Signal Flowchart

was displayed as a frequency reference on the CRO.

Essentially, three electronically independent instruments were used for signal recording. These were: displacement transducer, sound level transducer, and strain gauge transducer. All three were useful and practical. They are considered in turn.

Displacement Measurements - a fiber optic, non-contacting displacement transducer, the Fotonic Sensor, was used at the beginning of the experiment. Its use had to be discontinued later on because of the break-down of the instrument. Moreover, this particular instrument was unsuitable for the amplitude measurements around 10 KHz. The amplitudes were less than one angstrom in magnitude for the vibration levels involved in the experiment. The available instrument was simply not sensitive enough for amplitudes of vibration of that order.

Sound Level Measurements - these were recorded by means of a General Radio Sound level meter, type 1565-A. This instrument was used essentially for waveform recording and frequency reference. The sound level for the specimens fluctuated approximately twenty decibels, between the limits of fifty and one hundred and ten decibels; the instrument emitted a signal proportional to the sound level fluctuation over a range of ten decibels. In recording the sound pressure level, the signal was displayed either directly on the CRO, or on the level recorder. The sound pressure level frequency spectrum data turned out to be useless due to the background noise compounded with the noise emitted by the specimen and its reflections in the best room. No trend could be established. However, with the addition of an anechoic chamber, sealing off of the background noise and perhaps attenuating the reflections, such records might prove useful.

To establish whether the characteristic strain waveform at the resonant first and second longitudinal vibration of the bar and the resonant first and second radial vibration of the plate could be recorded independently, the sound level meter output was displayed simultaneously on the CRO. The microphone was suspended approximately four feet above the plate, and off center. For the bar, the microphone was suspended approximately six inches above the bar and over one cantilever. With this arrangement, the sound level meter recorded the net result at that point of all sound waves emanated and reflected from the specimen and surroundings.

Strain Gauge Measurements - on both the bar and the plate, strain gauges were applied in appropriate positions. These gauges were hooked up in suitable networks with, or without temperature compensating gauges in external half, or full bridges to the bridge amplifying meter. Since, in general, the strains measured were extremely small, less than 20 μin/in, high resistance wire strain gauges and 120 ohm film strain gauges temperature compensated for steel were used. In addition, dry cells were used in series with the internal excitation of the bridge amplifying meter to make the bridges as sensitive as was possible without overloading the electronic network. From the BAM, the signal was taken either directly to the oscilloscope, for qualitative and quantitative measurements, or the signal was amplified in another stage of amplification and then recorded on the level recorder. The last amplification mentioned was a necessity since the level recorder had a minimum signal level of 10 mv RMS, and the maximum signal recorded at the output of the BAM was less than 40 mv peak-to-peak.

Most instruments were hooked up for floating ground - grounding was done through the oscilloscope. The components grounded were: the power amplifier, the sound level meter, the Fotonic Sensor, the specimen, the

oscilloscope, and the block on which the dummy guages were mounted.

Individual Instruments

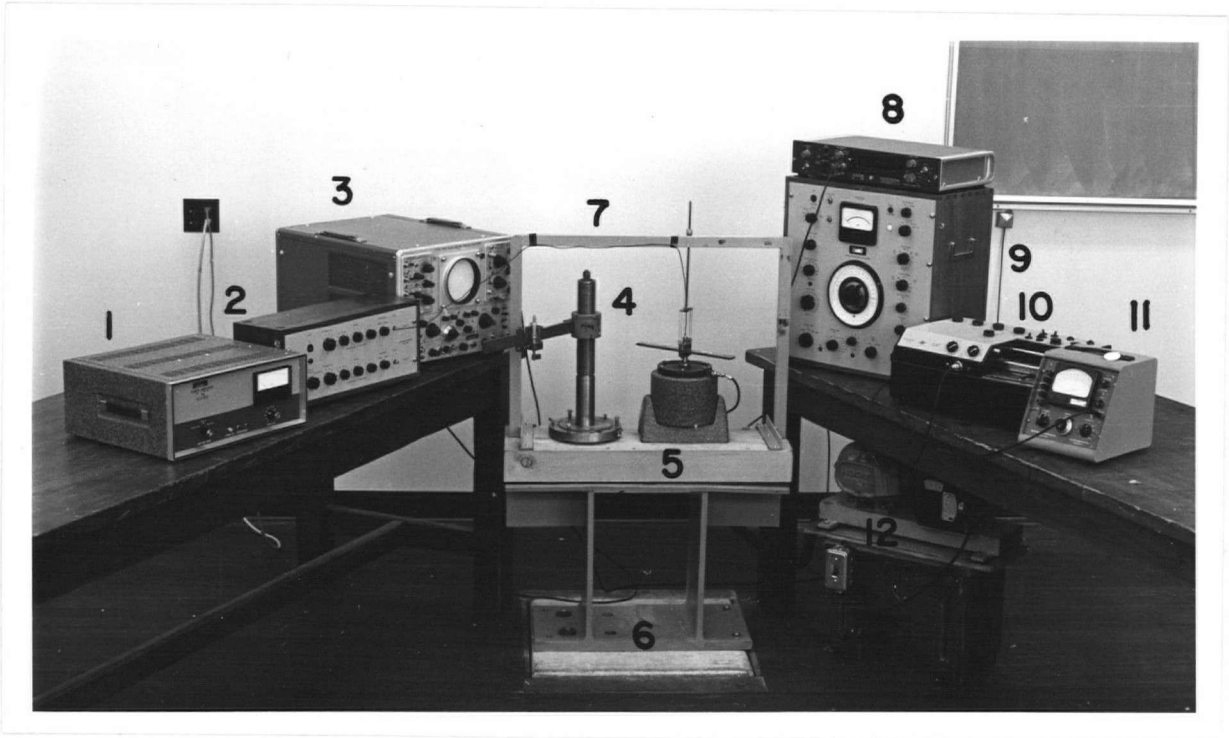

Fig. 4. Overall View of the Instrumentation

1 Power Amplifier
2 Amplifier
3 CRO
4 Polar Height Gauge
5 Electromagnetic Exciter
6 Test Bed
7 Frame
8 Frequency Counter
9 Control Unit
10 Level Recorder
11 BAM
12 Roots Blower

An overall view of the instrumentation set up is shown in Fig. 4. Not shown in the figure is the Fotonic Sensor, the storage oscilloscope, and the vacuum tube voltmeter.

With automatic control, the system can be operated from 10 Hz to 10,200 Hz. The maximum force available is 50 lbs; the maximum displacement of the plunger of the electromagnet is restricted to less than 0.5 inches peak-to-peak. The system can be run backward or forward, or backward and

forward continuously over the whole frequency range, or over segments of its range. The system can be run continuously at maximum power. The frequency sweep of the generator of the control unit can be synchronized with the frequency calibrated paper feed of the level recorder. The recording can be done over the full frequency range of the control unit; an average frequency reading can be obtained from a digital counter. Without automatic control, the frequency range can be extended from 10,200 Hz to 20,000 Hz, but at a reduced force. The manufacturer suggests an upper limit of 25 lbs. under these circumstances. Without automatic control, the control unit and the level recorder are taken out of the circuit. The output of an external function generator replaces the control unit. Under these conditions the controls revert to manual - this extension requires a lot of patience and attentiveness on the part of the operator.

The Bruel and Kjaer Automatic Vibration Exciter Control Unit Type 1025 provides a constant displacement control up to 2 KHz and a maximum amplitude of 0.1 in. peak-to-peak; constant velocity control is available up to 2 KHz and up to 100 in/sec peak value; constant acceleration control is feasible up to 10 KHz and 1000 g peak value (1 g ≡ acceleration of gravity). Since the frequency dial on the instrument was not properly calibrated, and even if it had been, it is impossible to read frequencies closer than 50 Hz at the upper end of the frequency scale, an external General Radio Company Digital Time and Frequency Meter, Type 1151-A, Serial 347 was used for frequency measurements. At low scanning speeds of the control unit, this unit provides not an instantaneous, but an average frequency. At steady state, it displays the true frequency of the excitation (provided the signal is stable and the $\pm$ 1 count inaccuracy has been taken into account). The control unit has six fixed scanning speeds if used with the synchronized level recorder,

or 132 scanning speeds otherwise. In terms of frequencies being swept out per unit of time, the concept of a fixed scanning speed has no meaning. This arises from the fact that the generator produces the frequencies logarithmically with time, whereas the scanning device is synchronous, or constant with time. The control unit has fixed or pre-programmed compressor speeds.

The Bruel and Kjaer Level Recorder, Type 2305, was synchronized electronically with the control unit for most tests. As plotting medium 50 mm wax paper, frequency calibrated, was used in conjunction with a sapphire pen and every plot was calibrated separately. This level recorder does not reproduce the instantaneous value of the function, but plots either the RMS, DC, or peak value. The RMS function was chosen for this experiment - the influence of sudden extraneous signals is minimized thereby. Different paper and writing speeds are available.

The Ellis Associates BAM 1 Bridge Amplifier and Meter has a DC amplifier whose frequency response is not flat over the used frequency range. At 10 KHz the attenuations is approximately 3%. A Hewlett Packard DC Vacuum Tube Voltmeter was used to measure the effective excitation voltage of the different bridges. The amplifier section of the Bruel and Kjaer frequency analyzer Type 2107 was used as cascading amplifier after the BAM unit.

The MB Electronics Model 2250 Power Amplifier is capable of delivering up to 400 watts of power to the exciter. The Bruel and Kjaer dual channel accelerometer preamplifier Type 2622 has a built-in sensitivity attenuator for setting of the accelerometer sensitivity. For correct setting of the accelerometer sensitivity, the channel output is scaled to 10 mv/g. The waveforms of interest in the experiment were displayed on the Tektronix 565 Dual Beam (or four beams with chopper) oscilloscope and photographed

therefrom. Finally, the polar height gauge and Fotonic Sensor probe holder was designed and built in the Department. These devices allow displacement measurements in three coordinates - θ, r, h.

Test Bed and Frame

The test bed on which the vibration exciter was mounted consisted of a block of wood, a steel casing, and a two foot by two foot block of concrete. The whole assembly was embedded in the ground beneath the floor of the laboratory. See Fig. 5.

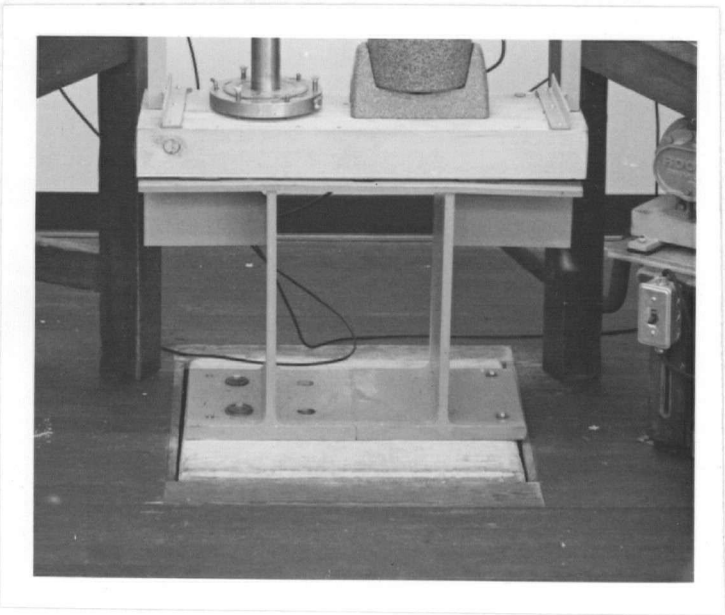

Fig. 5. Test Bed

The concrete block was structurally isolated from the building. Since the tests were carried out during the night, the influence of Rayleigh Surface waves (caused by trucks and cars passing the nearby road, unbalanced machinery inside the building) was minimized. The steel casing shown in the figure consisted of two heavy T-sections joined on the top by 1/2 inch steel plate, braced by two gussets, welded together, and bolted to the concrete block. A wooden block was screwed to the steel plate. This was used as a damper as

well as a support for the frame to which the suspension and auxiliary fixtures were attached. The frame running the full length of the working surface consists of a 3/16 x 1¼ inch angle iron, welded together and screwed to the wood. A hole was drilled through the angle iron directly above the center of the vibration exciter for attachment of the specimen suspension.

Suspension

For the plate as well as for the bar, an external suspension had to be provided to take the weight of the moving element, specimen, and any necessary appendages off the electromagnet. In the experiment, this was a necessity in order to obtain the level of acceleration used throughout the tests.

The suspension for the bar, shown in Fig. 6, consisted of two

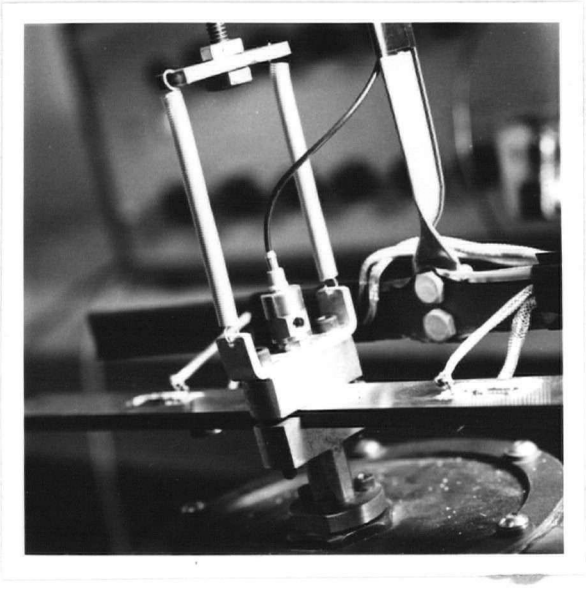

Fig. 6. Bar Suspension

spring systems in parallel. First, there was the spring action provided by an annular rubber diaphragm incorporated in the vibration exciter. Second, there was provided an external spring system consisting of coil springs. For

the plate this system comprised four springs in parallel; for the bar two springs were used in parallel. The criterion for the choise of springs was to keep the natural frequency of the complete spring-mass system as far away as possible from the lowest operating frequency. Without power flow to the exciter, a natural frequency between four and five cycles per second for both systems was attained with the available springs.

The suspension was attached to the frame via a long 1/4" threaded rod running through the hole in the upper angle of the frame. A hemispherical surface was machined on a large nut to keep the rod from sliding down and to support the weight to be suspended. This nut and a locking nut were threaded on the far end of the rod to an appropriate height. The hemispherical nut, resting on the hole in the angle iron, allowed for small misalignments of the moving parts in two orthogonal directions.

Plate Support

The plate was supported essentially, by a threaded shaft, one end of which had a wide flange which was bolted to the moving element of the electromagnetic exciter. The length of the shaft consisted of four types of thread - three external, one internal. The central external thread was a tapered pipe thread to match the pipe thread in the central hole of the plate. The internal one was used to fasten the accelerometer to the top of the shaft. The upper machine thread on the shaft was used to fasten the external spring system to the shaft.

Bar Clamp

The bar was clamped between two short cross beams, one of which was an integral part of a shaft arrangement as in the previous case. The accelerometer was threaded into the center of the upper bross beam; the lower wide flanged section of the shaft was bolted to the plunger of the exciter; the springs were attached to the upper cross beam. The double

cantilever bar arrangement was used to provide a balanced system on the shaker table.

Models and Boundary Conditions

Circular Plate

For the experiment a circular plate of mild steel, 1/4 x 16" dia. (nominal) was used. This diameter was chosen for the plate so as to bring the breathing mode frequency into the 8 KHz range. In the center of the plate a 1/4" pipe thread hole was machined. The surfaces were ground on a surface grinder and hand sanded to remove rust spots. Due to the grinding operation, the plate had assumed a curvature - insignificant to be considered a 'curved' surface.

The boundary conditions aimed for were: a circular plate without transverse load, free edges, and supported and excited in the center. As was mentioned under the heading 'Plate Support', the plate was supported by a threaded shaft. The section of the shaft with the pipe thread was screwed hand tight into the hole of the plate. The intention was to simulate a continuous plate, without a central hole. The Chladni figures obtained were to be an indication of the symmetry of the vibration.

Two other supporting conditions were considered. One, a solid plate clamped, or simply supported along its periphery; two, a clamped plate in the center. The first model was dismissed as impractical, considering the available excitation and the difficulty in producing the exact boundary conditions. The second one was tried. The plate was clamped between two nuts run up on the shaft and against the plate. In spite of the care taken in machining the surfaces involved, peculiar Chladni figures were obtained. Therefore, this boundary condition was abandoned.

Cantilever Bar

The bar was fabricated from 1/4 x 1" (nominal) cold rolled steel. The full length of the double cantilever bar was 12.38". This length was chosen so that the first coupled longitudinal resonant vibration occurred in the 8 KHz range. The cross beam width was 17/32". The surfaces were ground so as to remove surface pits.

The boundary condition to be simulated was that of two cantilever bars, obtained by clamping a single bar at the center with the cross beam. Obviously, the arrangement assumed will not yield true fixed end conditions. For bending, the boundary conditions were exact; for longitudinal wave propagation, the width of the cross beam has to be taken into account.

Strain Gauges and Bridges

Circular Plate

Two kinds of gauges were placed on the plate - for the tangential strains BUDD C6-141B film gauges of 120 ohm resistance were used; for the bending plus radial strain and the radial strain records 500 ohm gauges SR-4 CD-8 Baldwin Lima wound wire gauges were used. Identical gauges were used wherever dummy, or temperature compensating gauges were needed. The gauges were cemented to the surfaces with GA-1 and SR-4 strain gauge cement, respectively.

The location and hook-up of the gauges was as follows: Tangential - three gauges placed at random along the periphery and hooked up in series to form one arm of a 360 ohm external half bridge. The gauges were located as symmetrically as was possible about the central plane. Bending plus radial and radial strain - two gauges, of short filament length located within 1/64 of an inch from the outer edge. One gauge was located on each

side of the plate surface in corresponding positions. Two such gauge arrangements were placed at random along the periphery. For bending plus radial strain, two gauges on the same side of the plate were hooked up in series to form one arm of a half bridge. For radial strain records, a full 500 ohm bridge was connected with the active gauges, one on each side of the plate, connected so as to eliminate the bending strain. The location of the strain gauges in the radial direction was arbitrary since an optimum position for all frequencies could not be determined.

Cantilever Bar

Four BUDD C6-141-B gauges were located in symmetrical locations relative to the cross beam on both cantilevers. One gauge was located on the top surface and one on the lower surface in corresponding positions on each cantilever. The gauges were located 3¼" away from the end and equidistant from the sides. GA-1 cement was used for their adhesion. Because of the higher strain level involved, the gauges were hooked up into 120 ohm half bridge for the bending plus radial strain record and into 120 ohm full bridge for the radial strain record.

Bridges

As far as it was tolerable, additional external excitation of the bridge was provided. The criterion for the choice of magnitude of the external excitation was dictated by the available sources and the dissipative capacity of the strain gauges. As suggested by their respective manufacturers, 25 ma. was taken as the limiting current for the SR-4 gauges and 5 watts per square inch of grid area was taken as the limiting power for the C-6 gauges.

CHAPTER IV

TESTING

Calibration and Check Out

The accelerometer used in the experiment was calibrated at the factory. No calibration check was made prior to the experiment. The only test done was to compare its behaviour against a similar unit. Their outputs agreed reasonably well over the full frequency range. The influence of a cooling medium on the output of the accelerometer was examined. No appreciable differences were recorded.

The system as a whole and its individual components were checked as far as this was possible. The acceleration as set on the control unit, and the acceleration recorded by the accelerometer agreed exactly. The set point acceleration was not always constant throughout the different frequency ranges. The acceleration meter on the control unit indicated small deviations from the set point. In general, these deviations were unpredictable and insignificant. The oscilloscope's calibration was checked prior to the experiment. The frequency response of the BAM was checked. The frequency response complies with the manufacturer's specification. The frequency response of the cascaded amplifier (amplifier of the frequency analyzer) was checked. Its response is flat over the frequency range involved. For the particular application, an external frequency counter in conjunction with the control unit was a necessity. Frequencies cannot be read from the control unit frequency scale closer than approximately 250 Hz at 10 KHz. In addition,

the frequency scale was not properly adjusted, or calibrated. The required airflow through the electromagnetic exciter was checked at maximum, constant power dissipation. The airflow rate and the power input to the compressor were inadequately specified by their respective manufacturers. A doubling of the first quantity and tripling of the second quantity was necessary. The cooling system as now designed is adequate for continuous service at full power dissipation. The synchronization between the level recorder and the control unit was good.

The natural frequency of the complete suspension of the system was established. To determine this frequency, a storage oscilloscope and the Fotonic Sensor plus the height gauge were used. The probe of the Fotonic Sensor was suspended over the surface of the plate, and the dynamic output of the instrument was displayed on the storage oscilloscope. Finger pressure was used to drive the system (specimen, adapters, plunger, accelerometer) at its natural frequency. This procedure was repeated several times, and the average of the recorded frequencies was taken. The deviations from the mean were very small.

Noise problems arising from ground loops were eliminated. All cables and wires used were shielded. Electromagnetic pick-up was minimized.

Test Procedure

Since the test procedure for the plate is similar to that of the bar, only one is described below. The plate with strain gauges and lead wires attached was bolted to the plunger of the electromagnet, making use of the appropriate adapter. The connector for the suspension and the accelerometer was attached. By means of a centering nut, a string, and a plumb,

the exciter was centered directly under the hole in the frame. The suspension was attached to the frame, as outlined earlier, and the whole assembly was lifted by means of the hemispherical nut until the specimen, adapters, etc. vibrated with the least excitation. This required a trial and error procedure. Next, the stay ring was attached to the frame, and the lead wires to it. By the procedure indicated earlier, the natural frequency of the system (specimen, adapters, accelerometer, and plunger of electromagnetic exciter) was determined. Next, the active gauges and the temperature compensating gauges were checked for their resistance; the gauges were combined in the proper order to form the desired circuits and then connected to the appropriate posts of the BAM. The shields of the lead wires and the ground wire of the specimen and the temperature compensation gauge block were connected to the ground of the oscilloscope. The external excitation was added to the BAM. All instruments were properly interconnected, and connected to the power source. Then the instruments were turned on and left in the stand-by position for at least two hours.

The next phase of the test procedure was to determine the specimen characteristics - what acceleration to use over which frequency range. This required a trial and error procedure. The figures in Table 1 were found to be satisfactory for the plate and the bar, respectively. This tabulation is useful in later discussions.

The actual testing got under way after:
(a) setting the set point acceleration, (b) synchronizing the level recorder with the control unit, (c) choosing the scanning speed and direction, (d) determining the compressor speed, (e) choosing the attenuation, the writing speed, and the type of response of the level recorder, (f) cooling the exciter with forced air, and (g) calibrating the BAM and measuring the

Plate Characteristics			Bar Characteristics		
Frequency Range Hz		Maximum Acceleration g	Frequency Range Hz		Maximum Acceleration g
150	200	2	400	1000	40
200	700	5.5	1000	1200	20
700	800	0.5	1200	1500	1.4
800	1000	4.5	1500	3600	50
1000	1500	30	3600	4000	7
1500	2000	26	4000	7000	100
2000	2400	3	7000	7500	14
2400	7000	110	7500	9500	100
7000	7400	15	9500	10000	60
7400	10000	80			

Table 1. Allowable Acceleration Level

excitation voltage of the bridge. Since each test extended over long periods of time, the last step had to be done periodically during the course of the experiment. The high external voltage source's life was limited - up to 50% reduction in excitation was encountered.

Constant Power Plot Discussion

The ideal approach to the experiment would have been, of course, a constant displacement frequency sweep of the specimen. A practical example explains best this choice. A rotating shaft to which a circular disc is rigidly attached is considered. If the bearing in which the shaft is rotating is misaligned, so that the disc experiences a sinusoidal transverse periodic excitation, according to the theory proposed herein, two radial vibrations of the disc and the associated radial resonant vibrations must be expected. Since the axial displacement of the shaft can be considered constant, regardless of the frequency of rotation, an investigation, assuming the above

criterion, is highly desirable. As was stated in the description of the overall system, such an investigation was not possible.

The next best test procedure would have been a constant power plot, however, the system is not designed for this kind of control.

The next alternative was a constant acceleration control. This kind of control was also unsuitable. Since the frequency sweep extends from 100 Hz to 10 KHz, it can be shown that the peak amplitudes in the center of the plate are drastically reduced, by a factor of 10^4, and, consequently, the resulting strains are very small, perhaps too small to be distinguished from the inherent electronic noise. This point is clarified by the two charts below, Fig. 7.

(a)

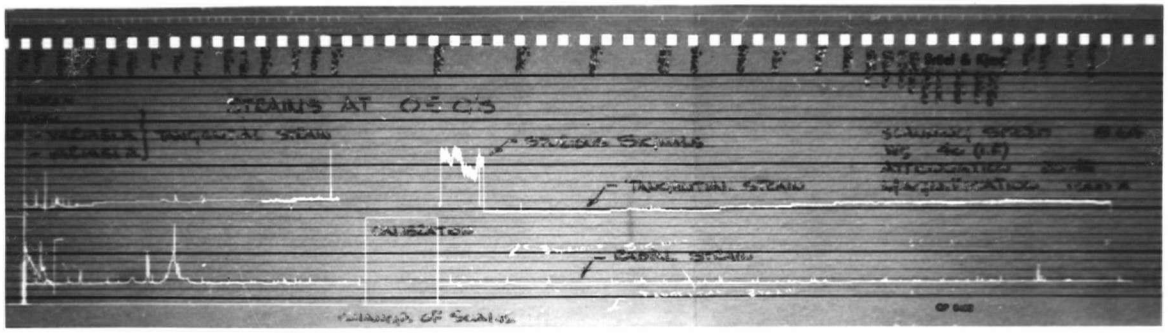

(b)

Fig. 7. Constant Acceleration and Approximated Constant Power Frequency Spectra

(a) Constant acceleration

(b) Approximated constant power

In Fig. 7(a) the constant acceleration plot for the plate is shown, for both radial and tangential strain. Only one resonant vibration (tangential strain at 4405 Hz) shows up clearly. In Fig. 7(b) the approximated constant power frequency spectra for the plate is shown. Two resonant vibrations, one at 4405 Hz and one at 8810 Hz, can be identified clearly. The additional information obtained from the approximated constant power plot dictated its choice over the constant acceleration control.

By definition, the approximated constant power frequency spectra is the break-up of the full frequency spectrum into a number of convenient, small segments along which the acceleration is kept constant; different acceleration levels are used for different segments such that at one point of each segment, the power input to the plate is a maximum (170 watts approximately). The number of segments and their location is an engineering decision - an optimization process. Table 1 lists these frequency segments and the constant acceleration level. This procedure allows for the fact that the maximum allowable acceleration level of the specimen plus its adapters, is lowest at the resonant frequencies. This procedure results in an optimum testing, considering all the factors involved. This procedure allows the constant acceleration control facility of the system to be used. This procedure results in a decrease in amplitude of vibration by only a factor of 10^2 as compared to 10^4 for a constant acceleration frequency spectra between the frequency extremes. This procedure is the first approximation to a constant, maximum power frequency spectra.

The frequency response spectra, as will be shown shortly, were plotted in a particular manner to satisfy two conditions. First, the different frequency segments were separated from each other. This was a necessity since transient voltages were set up whenever certain controls

were changed. For instance, in changing the acceleration level, the scriber of the level recorder had to be lifted off the paper. Further, since different acceleration levels resulted in different locations of this trace, different attenuation of the signal at the level recorder was used for different frequency segments. Second, since the damping is small in steel, the resonant vibrations do show up as spikes in the records. To make absolutely sure that none of these spikes were missed, sufficient frequency overlap was provided. This was achieved by running the whole system 'backwards', approximately 50 - 100 cycles and then forward again, after having decided on a new attenuation level.

Interpretation of Frequency Spectra

All frequency spectra shown herein were obtained by magnifying the strain gauge signal in the BAM 120 x (depends slightly on the frequency) and 1000 x thereafter in the cascaded amplifier. To correlate the trace on the record with the measured strain, the following must be known:

(a) the bridge excitation used at that time (this variable is a function of time),

(b) the bridge arrangement and the gauge factor,

(c) the acceleration level in this particular frequency range, and

(d) the attenuation of the level recorder.

Because the translation of the voltage level into a true strain record is a tedious one, and because the aim of this thesis is to show only the existence of the predicted vibrations, no such translation was carried out. The only strain calculations carried out were at the predicted longitudinal resonant vibrations of the bar and at specific frequencies close by. The purpose was to show the significance of this resonant vibration.

Chladni Figures

The Chladni figures reproduced herein were obtained by uniformly distributing ordinary sugar on the plate. The exact transverse resonant vibrations were established in the following manner. The first indication of a resonant transverse vibration was obtained from the sugar - the individual sugar grains moved to a nodal circle. An even closer approximation could be obtained by observing the output voltage of the exciter control unit. As a narrow frequency range straddling a transverse natural frequency was swept through, the output voltage suddenly swung to a high value, and then fell off again. The method used to obtain the figures listed herein is as follows. The probe of the Fotonic Sensor was suspended over the specimen, at a fixed position, and its output, at a constant setting, was displayed on the storage oscilloscope. A frequency response survey was made, at discrete frequencies, through the expected range. At the frequency where a natural frequency occurs, a maximum response was recorded on the oscilloscope.

Plotting and Photography

The plotting was done on frequency calibrated, 50 mm, logarithmic, wax paper. A sapphire stylus was used as scriber. This combination resulted in a very high resolution of the signals. Ink on ordinary paper would have been easier to reproduce, however, the resolution of this combination is not as good.

The appended photographs of waveforms, Fig. 10 and Fig. 11, were taken directly from the screen of the Tektronix oscilloscope, in the single sweep mode, with a Pentax camera and Tri-X film.

CHAPTER V

EXPERIMENTAL RESULTS

In this section the experimental findings are presented. An interpretation and a discussion of the same is presented in Chapter VI. To make the discussion coherent, all the findings of the plate are presented first, followed by those for the bar.

Circular Plate

Figure 8 shows the Chladni figures for the transverse resonant vibration of the plate, second to fifth natural frequency.

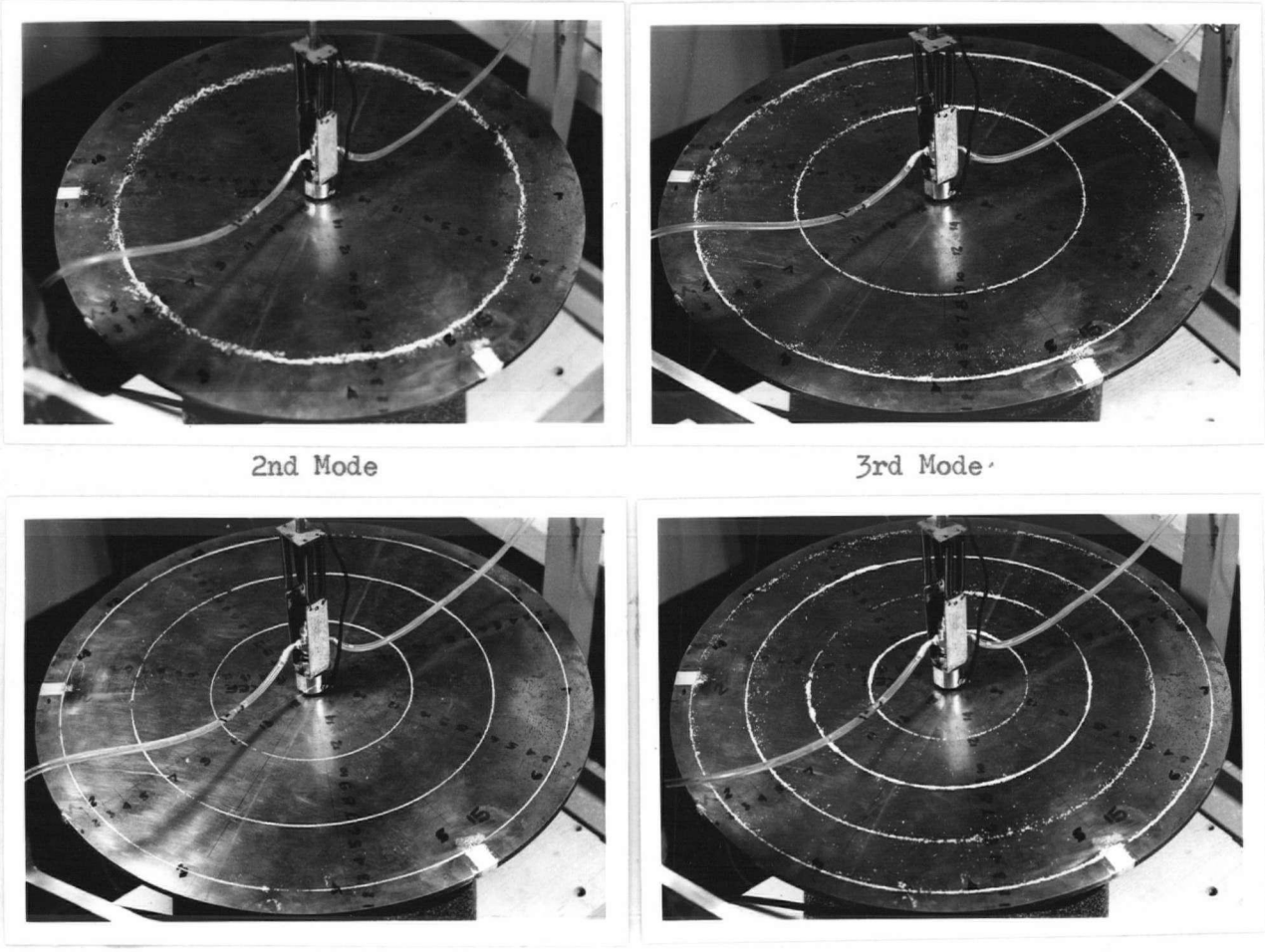

2nd Mode

3rd Mode

4th Mode

5th Mode

Fig. 8. Chladni Figures for the Transverse Vibration of the Circular Plate

For photographic purposes, more sugar than was actually needed was oscillating on the plate. The resolution can be improved above that shown in the figure.

The natural frequencies of transverse vibration of the plate, and the non-dimensionalized nodal radii, with their respective largest deviation from the mean radius, are shown in Table 2. The natural frequencies serve as a test for the boundary conditions; the largest deviation from the mean radius is a measure of the symmetry of the vibrating system.

Mode	Frequency Hz	Non-Dimensionalized Mean Nodal Radii				Largest Deviation from Mean Radius
		1	2	3	4	in
2	767					
3	2204	0.87	0.51			0.02
4	4335	0.91	0.65	0.36		0.03
5	7130	0.93	0.73	0.50	0.28	0.04

Table 2. Non-Dimensionalized Nodal Radii for Plate

Note: The average deviation is much smaller than the values quoted above. The non-dimensionalized nodal radii are based on a full radius (plate without a central hole).

The mean nodal radii were determined by averaging three random radius measurements. The frequencies quoted above were measured with the digital counter during steady-state vibration. The errors and inaccuracies involved in the frequencies quoted are:

(a) experimental error arising from inaccurate location of the resonant peak - less than 1 Hz,

(b) the round off error from the fourth and fifth digit, and

(c) inherent inaccuracies of the counting device.

In Appendix C, Fig. C-14 to Fig. C-16 are shown three 'approximated constant power' frequency spectra for the plate. Two spikes in the radial strain record and the tangential strain record, Fig. C-15 and Fig. C-14, are shown. The first occurs at 4405 Hz and the second at 8810 Hz.

There is one limitation inherent in the frequency spectra. Incorporated in these records is a contribution from the electromagnetic induction in the gauge installation. In the experiment, this extraneous signal was minimized. However, it could not be eliminated. The signal impressed by this electromagnetic induction has always the frequency of the excitation. For the resonant peaks, their influence is small (approximately 5% of the amplitude for the fundamental longitudinal frequency); at other excitation frequencies this signal is very significant. Care must be exercised, therefore, in interpreting the spectral records.

Fig. 10 depicts the waveforms at the two radial resonant vibration of the plate. Their interpretation is given in Appendix A.

Cantilever Bar

Figure 9 shows the Chladni figures for the transverse vibration of the bar.

Next, the natural frequencies for the transverse vibration and the non-dimensionalized nodal distances from the built-in end are tabulated.

The frequencies indicated in Table 3 have the same limitations as the measured frequencies for the plate. The resonant frequencies were measured to check the assumed boundary conditions.

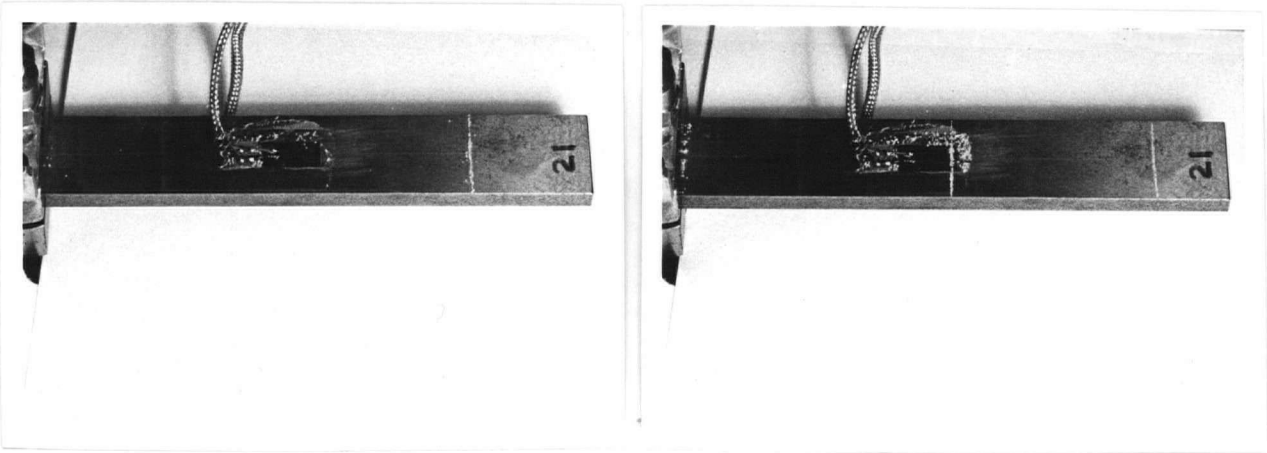

2nd Mode 3rd Mode

Fig. 9. Chladni Figures for the Transverse Vibration of the Cantilever Bar

Mode	Frequency Hz	Non-Dimensionalized Nodal Distances from the Built-in End	
		1	2
2	1367	0.78	
3	3805	0.50	0.86
4	7364		

Table 3. Non-Dimensionalized Nodal Distances for the Bar

Note: The nodal distances for the fourth mode could not be measured. The nodal lines are poorly defined at 7364. Further, all non-dimensionalized nodal distances were calculated using the exposed length of the bar as reference length.

The 'approximated constant power' frequency spectra for the bar are shown in Appendix C, Fig. C-17 and Fig. C-18. The two resonant longitudinal vibrations are clearly labelled in the axial strain record, Fig. C-18. Expected locations of higher vibrations than twice the frequency

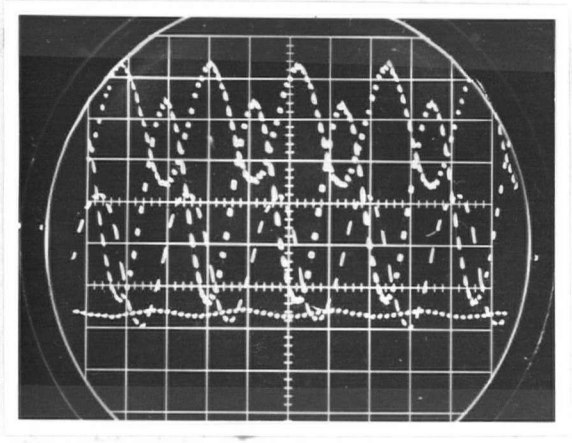

Breathing Mode

(a) Frequency 8810 Hz

Signal Order (top to bottom)
Radial Strain
Tangential Strain
Acceleration
Displacement

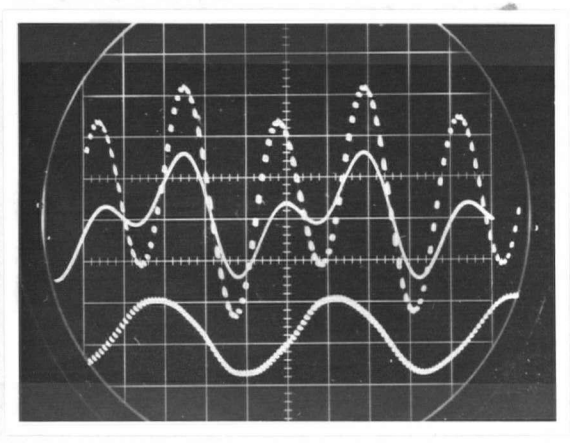

(b) Frequency 4404 Hz

Signal Order (top to bottom)
Bending and Radial Strain
Sound Pressure
Acceleration

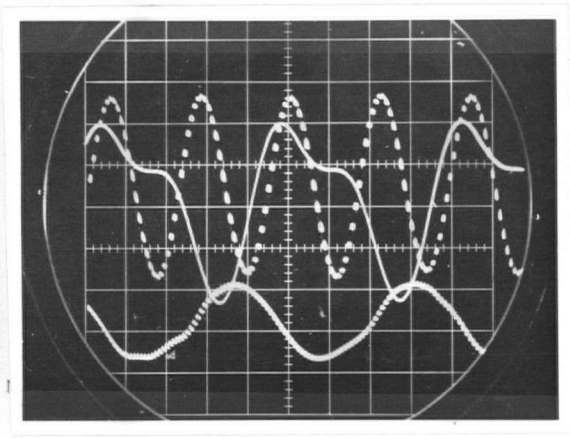

(c) Frequency 4403 Hz

Signal Order (top to bottom)
Radial Strain
Sound Pressure
Acceleration

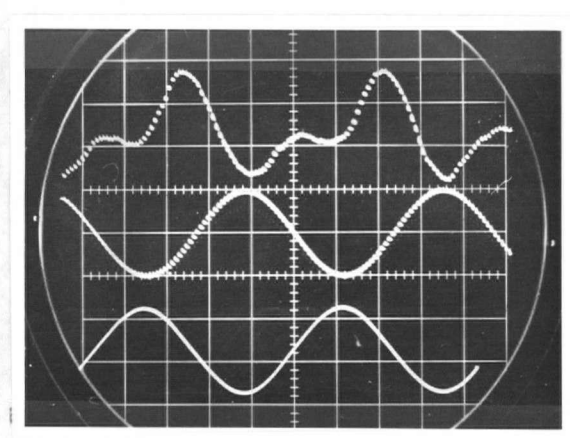

(d) Frequency 4405 Hz

Signal Order (top to bottom)
Tangential Strain
Sound Pressure
Acceleration

Fig. 10. Waveforms at Resonance for Circular Plate

of the excitation are indicated as well as the expected transverse coupled vibrations.

In Fig. 11 are shown typical waveforms at the resonant transverse vibration.

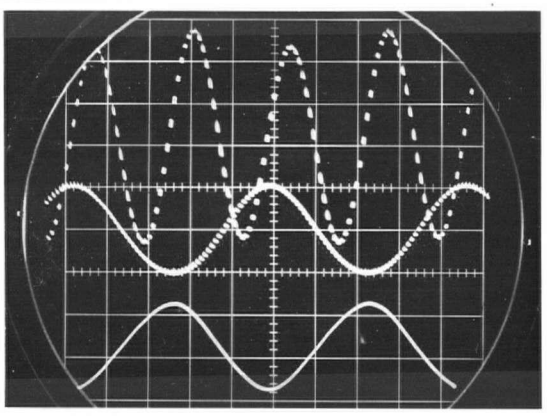

2nd Longitudinal Vibration

Frequency 4135 Hz

Order of Signals (top to bottom)

Longitudinal Strain
Sound Pressure
Acceleration

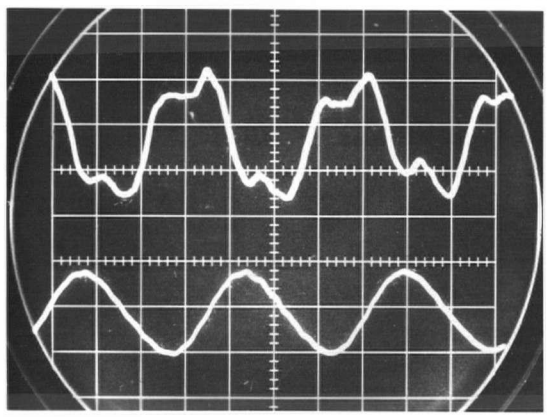

3rd Longitudinal Vibration

Frequency 2756 Hz

Order of Signals (top to bottom)

Longitudinal Strain
Acceleration

Fig. 11. Waveforms at Resonance for Cantilever Bar

CHAPTER VI

DISCUSSION OF EXPERIMENTAL RESULTS

Circular Plate

Table 4 lists the theoretical resonant frequencies for the transverse vibration.

Mode	Frequency Hz
2	700
3	2030
4	4000

Table 4. Theoretical Resonant Frequencies for the Transverse Vibration of the Circular Plate

Comparing this data with the data in Table 2, great differences in the frequencies are observed. The difference in frequencies suggests that the boundary conditions aimed for could not be realized. Further, the theoretical frequencies in Table 4 are based on a plate with a free edge and supported in the center. The experimental frequencies listed in Table 2, however, are based on a plate with a free edge and 'clamped' in the center over a small area. For transverse vibration, the small 'clamping' area results in a stiffer plate than a plate clamped strictly in the center. The higher frequencies in Table 2 as compared to those in Table 4 seem, therefore, to be justified.

The calculation for the breathing mode (assuming a solid plate) indicates a radial resonance at 8900 Hz. The measured resonant radial vibration frequency was 8810 Hz. For the radial vibration, a plate with a discontinuity in the center, in the form of a circular hole, is a less stiff structure than a plate without a hole. Therefore, it is to be expected that the natural frequencies for radial vibration will be lower.

The largest deviation from the mean radius of the nodal radii, Table 2, are relatively small. Consequently, the vibration was nearly symmetrical with respect to the center, or no gross singularities existed in the plate with exception of the center.

The static maximum deflection of the plate was determined to be $7.18 \times (10)^{-4}$ inches. In addition to this deflection, there existed the deflection due to the initial crookedness of the plate. The dynamic deflections were, in general, much smaller than the static deflection.

The tangential strain record, Fig. C-14, shows two pronounced peaks - one at 4405 Hz and one at 8810 Hz. Another at 1160 Hz cannot be explained. No other significant peaks were found. The radial plus bending strain record, Fig. C-16, shows also these two spikes in addition to the resonant bending peaks. It is important to note the difference in shape of the two peaks - the bending resonant strains do not build up as fast as the radial resonant strains. Also, it is worthy to examine the lower radial resonant peak in these figures. First, one sees from Table 2 that the fourth mode of flexural vibration occurs at 4335 Hz; second, the radial vibration occurs at 4405 Hz. The spike is just to the right of the peak bending strain and is indeed approximately of the same magnitude. However, since the gauge was not located at a position of maximum bending strain, it must be concluded

that the radial resonant strain is smaller than the bending strain at resonance. The radial strain, Fig. C-15, record corroborates these statements. Two peaks, at 4405 Hz and 8810 Hz respectively, corresponding to the radial resonant vibration, are indicated. In addition, vestiges of all the bending resonant strains are visible. The explanation for this might be, one, an incomplete compensation of the gauges and, two, the influence of the bending strain on the longitudinal vibration.

Next, the waveforms involved are examined. The radial and the tangential strain waveforms, at 8810 Hz, are shown in Fig. 10. The waveforms are periodic and of the same frequency as the excitation. Therefore, at 8810 Hz a resonant radial vibration, the 'breathing mode', exists. Figure 10 (b), (c), and (d) represent, respectively, the bending plus radial strain, the radial strain, and the tangential strain. Appendix A has to be consulted for their interpretation. It is seen that the signal is essentially the superposition of two harmonics - one of the frequency of the excitation, and one twice that frequency. The waveform recorded by the sound level meter is the same as that of the strain signal.

Cantilever Bar

The theoretically determined nodal distances for a cantilever beam, excited at the built-in end, are listed in Table 5.

Mode	Non-Dimensionalized Distances from the Built-In End		
	1	2	3
2	0.783		
3	0.504	0.868	
4	0.358	0.644	0.906

Table 5. Non-Dimensionalized Theoretical Nodal Distances for a Cantilever Beam

In Table 6 are listed the theoretical resonant frequencies for the transverse vibration of the beam as well as estimates of the maximum error (upper bound) for the calculated frequencies. The upper bound error estimates take into account the inaccuracies in the measurements of the physical properties and parameters of the bar.

Mode	Theoretical Frequency Hz	Maximum Error Hz
2	1400	148
3	3860	406
4	7550	795

Table 6. Theoretical Resonant Frequencies for Flexural Vibration of the Beam

The predicted resonant frequencies for flexural vibration listed in Table 6 were derived from the cantilever beam frequency equation. Not listed are the predicted resonant frequencies for flexural vibration for a cantilever plate. These frequencies are somewhat higher than those listed in Table 6. The actual resonant flexural frequencies of the bar, Table 3, are lower than those in Table 6. However, comparing the frequencies in Table 3 with those in Table 6, taking into account the upper bound on the error, one must conclude that the agreement between the two sets of data is reasonable. It seems that the bar behaved more like a beam than a plate.

The agreement between the measured non-dimensionalized nodal distances from the built-in end, Table 3, and the theoretical nodal distances from the built-end tabulated in Table 5 is good. This corroborates the conclusion arrived at in the previous paragraph.

The theoretically predicted first coupled resonant longitudinal

vibration should occur at 8520 Hz. if it is assumed that the effective length of the bar is its exposed length. If the half length of the full double bar is considered, the first coupled longitudinal resonant vibration ought to occur at 8150 Hz.

Comparing this data with the experimental findings, a discrepancy is observed in the first coupled longitudinal resonant vibration frequency. This suggests that the boundary conditions aimed for could not be realized. In considering the longitudinal vibration, the effective length of the bar is not its exposed length, but it includes an additional length under the clamp.

Examining next the strain records, the following observations are made. Axial Strain - as can be seen from Fig. C-18, there is a pronounced spike at 8270 Hz, the first coupled longitudinal resonant vibration, and one at 4135 Hz excitation, the second coupled longitudinal resonant vibration. Further, there is a very, very small spike at 2755 Hz labelled A_4. No others can be identified positively. Also, as for the plate, Fig. C-14, one sees vestiges of the flexural strain resonant vibrations. These must be interpreted in the same light as those for the plate. Bending plus Axial Strain - in Fig. C-17, there is a pronounced spike at 8270 Hz and one at 4135 Hz excitation. None can be seen at 2755 Hz. As before, the resonant longitudinal strain is at most equal in magnitude to the resonant flexural strain. In the same spectra, one sees the flexural resonant peaks. Again, one notes that the flexural resonant vibrations build up much more slowly than the longitudinal resonant vibrations. One other item in these spectra is worthy of note - spikes labelled A_1 and A_3. The first one occurs at one-half the frequency of the excitation of the second bending resonant mode; the second one occurs at one-half the frequency of the excitation of the fourth resonant

bending mode. Both peaks are extremely small compared to the strains just prior and just after its occurrence and both peaks show the characteristic slow build-up of bending resonant strains. The signals involved are too small for an accurate waveform analysis. However, by analogy with the more pronounced longitudinal coupled vibration findings, it can be assumed that these represent flexural vibrations of the bar at twice the frequency of the excitation. In other words, these small peaks represent the influence of the longitudinal coupled vibration on the flexural vibration as indicated in the theory by the term $(U_x \bar{W}_x)_x$.

Examining next the waveforms at the three significant spikes for longitudinal vibration, Fig. 11, making use of Appendix A, one has to conclude the following: at 8270 Hz excitation, a longitudinal resonant vibration of frequency 8270 Hz exists; at 4135 Hz excitation a longitudinal resonant vibration of frequency 8270 Hz exists; at 2755 Hz excitation a longitudinal resonant vibration of frequency 8270 Hz exists.

CHAPTER VII

SUMMARY AND CONCLUSION

Suggestions for Future Research

Besides the obvious research to be done, such as the analytical solution of the exact formulation, a number of experimental investigations based on the predictions of the simple, proposed formulation can and should be done. The relationship between response and excitation should be examined. This investigation can be done with the present set up. Next, this research should be extended to the upper end of the acoustic frequency range. The damping of the transverse and longitudinal vibration should be investigated. Quantitative answers should be found for the influence exerted on the amplitudes and frequency response by viscoelastic and elastic-viscoelastic damping layers on the surfaces of the bar. Optimizing parameters for the viscoelastic and elastic-viscoelastic damping layers should be found. The isolation properties of these materials at the frequency range encountered should be investigated. Their transmission-of-energy properties are of interest. Conventional viscoelastic materials should be investigated 'in situ' and other promising materials should be evaluated. The surface treatment of the bar, or plate, for a particular damping material must be determined. The fatigue and temperature dependence of viscoelastic layers must be investigated.

The instrumentation can be refined. If possible, a control unit for constant displacement control up to the upper end of the acoustic frequency range should be acquired - the control technique adopted for this

research is not the best one. For further investigations, a Fotonic Sensor should be available. This instrument is the most promising one for waveform investigations - noise problems associated with the other two sets of measuring instruments are eliminated hereby. It is suggested that in the future, strain gauges designed explicitly for dynamic application be used. Time and capital outlay can be saved thereby. The BAM 1 should be altered to a BAM 2 through the acquisition of a suitable Ellis Associates amplifier. The frequency response of the present unit is down approximately 3% at 10 KHz. An amplifier of suitable gain and frequency response should be designed to replace the amplifier of the frequency analyzer. This unit should be available for its intended purpose. An anechoic chamber should be installed and its acoustic characteristics be studied. The General Radio Sound level meter should be replaced by an instrument having a wider linear range. A band pass filter should be incorporated into the system. The band should be synchronized to the sweep control of the generator. The desired boundary conditions should be approximated more closely. The arrangement used for the cantilever bar seems to be more promising than the support for the plate. A technique to evaluate damping materials should be determined.

Summary

The underlying reason for doing this experimental work was to verify the speculation that the transverse excitation of a beam leads to longitudinal vibrations of the beam. To this effect, a simplified model was set up. Assuming strains in the central plane, coupled nonlinear partial differential equations of motion were derived for a beam. By suitably manipulating the equations and interpreting some of the coupling terms, two coupled longitudinal vibrations, with a frequency ratio of 1:2, were predicted. In addition, two coupled flexural vibrations, with a frequency ratio of 1:2,

were anticipated.

The experimental investigation proved the validity of the above predictions. Two resonant longitudinal vibrations were determined for a bar and the frequency ratio was 1:2. Further, through the investigation, the location of the resonant peaks in regards to the frequency of the excitation was established. The first longitudinal resonant vibration occurred at the fundamental frequency for longitudinal resonant vibration. The second longitudinal resonant vibration occurred at 1/2 times the frequency of the transverse excitation at the fundamental frequency for longitudinal resonant vibration and the frequency of the vibration was that of the fundamental longitudinal resonant vibration.

Also, one longitudinal vibration at three times the frequency of the excitation in the transverse direction was recorded. The frequency of the vibration seemed to be that of the fundamental longitudinal resonant vibration. In the strain records there is evidence that there are more flexural resonant vibrations than indicated by the linear theory. These occur at one-half the frequency for flexural resonant strains. A waveform analysis was not carried out since the signal involved is very small.

Some general conclusions can be drawn in regards to the relative value of the magnitudes at resonance between the flexural vibration and the longitudinal vibration. At best, the longitudinal strain at resonance equals the bending plus longitudinal strain for transverse resonance; in general, it is smaller. Further, it seems that the magnitude of the strains at resonance decreases as the order of the longitudinal frequency increases.

An experimental investigation, analogous to that of the bar, was carried out for a circular plate suspended in the center and excited

transversely. Two coupled resonant vibrations in the radial direction were recorded. Their frequency ratio was 1:2; they occurred respectively at 1 and 1/2 times the frequency of the transverse excitation for the fundamental frequency for radial resonant vibration. No nonlinear coupled flexural vibration at one-half the frequency of resonant flexural 'linear' vibration were identified.

Conclusion

From the investigation, the following conclusions were drawn:

(1) The anticipated longitudinal vibrations exist, when a bar is excited transversely.

(2) There is some evidence that the anticipated flexural vibrations of the beam at twice the frequency of the excitation exist. Their influence, however, on the transverse vibration, even at their resonant condition, was extremely small.

(3) The derived differential equations of motion for the beam are correct insofar as the predictions of frequencies of coupled vibration are concerned.

(4) The method used in interpreting the special coupling terms is correct.

(5) Experimentally, it was determined that higher longitudinal vibrations than the second do occur. A third resonant longitudinal vibration was recorded.

(6) Resonant vibrations occur at the inverse ratio of their frequencies. That is, for the beam, the longitudinal vibration frequency ratio is 1:2, the resonant longitudinal vibrations occur respectively at 1 and 1/2 times the transverse excitation at the fundamental longitudinal resonant vibration.

(7) It seems that, at best, the amplitude for resonant longitudinal vibration

strain equals the amplitude for resonant axial plus bending strain. In general, it is smaller. Nevertheless, the amplitude for resonant longitudinal vibration strain is larger than the amplitude for longitudinal plus bending strain at near-by non-resonant condition.

(8) The longitudinal resonant strains build up much faster than the flexural resonant strains.

(9) For the plate, two radial coupled vibrations were recorded. Their frequency ratio was 1:2; they occurred at 1 and 1/2 times the transverse frequency for the breathing mode.

BIBLIOGRAPHY

1 Harris, C.M. and Crede, C.E., "Shock and Vibration Handbook", vol. 1, McGraw-Hill Book Co., N.Y. 1961.

2 Jacobsen, L.S. and Ayre, R.S., "Engineering Vibrations", McGraw-Hill Book Co., N.Y. 1958.

3 Love, A.E.H., "A Treatise on the Mathematical Theory of Elasticity", 3rd ed., Cambridge, University Press, 1920.

4 McLeod, A.J. and Bishop, R.E.D., "The Forced Vibration of Circular Flat Plates", Mechanical Engineering Science, monograph no. 1, The Institution of Mechanical Engineers, London, March, 1965.

5 Mettler, E., Dynamic Buckling, "Handbook of Engineering Mechanics", 1st ed., Fluegge, W., editor, McGraw-Hill Book Company, Inc. 1962.

6 Pearson, K., "Memoir on the Flexure of Heavy Beams Subjected to Continuous Systems of Load", Quarterly Journal of Pure and Applied Mathematics, vol. 24, Longmans, Green, and Co., London, 1890.

7 Pearson, K., and Filon, L.H.G., "On the Flexure of Heavy Beams Subjected to Continuous Systems of Load", Quarterly Journal of Pure and Applied Mathematics, vol. 31, Longmans, Green and Co., London, 1900.

8 Strutt, J.W., Lord Rayleigh, "Theory of Sound", vol. 1 and 2, Dover Publications, N.Y., 1945.

9 Thomson, W.T., "Vibration Theory and Applications", Prentice-Hall, Inc., N.J., 1965.

10 Timoshenko, S. and Woinowsky-Krieger, S., "Theory of Plates and Shells", McGraw-Hill Book Company, Inc., N.Y., 1959.

APPENDIX A

ADDITION OF TWO SINUSOIDS

In this section, analytical expressions are derived and graphical interpretations shown for the addition of two sinusoids of different amplitude, different frequencies, and in phase such that both functions cross the time axis at the same instant of time, and that an instant later both functions are either positive, or negative.

Part 1

Different amplitude

One frequency being twice the other

In phase

We consider the function

$$\begin{aligned} V &= A \sin \theta + B \sin 2\theta \\ &= (A + 2B \cos \theta) \sin\theta \\ &\equiv (\text{Modulated Amplitude})(\text{Circular Function}) \end{aligned} \tag{16}$$

Equation (16) represents a modulated amplitude rotating at the frequency of the fundamental function, that is, regardless how large the individual amplitudes are, the resulting waveform has one period equal to that of the fundamental function.

The maxima and the minima of the resulting function are found from

$$\frac{\cos 2\theta}{\cos \theta} = - \frac{A}{2B} \tag{17}$$

and $$\frac{d^2V}{d\theta^2} = - 4B \sin 2\theta - A \sin \theta \qquad (18)$$

As good as the above approach is, it does not afford an easy evaluation of the function (17) and (18) above. For this reason, the graphical evaluation of the original function is shown in Fig. 12. Everything which has been derived above, analytically, can be verified in these figures.

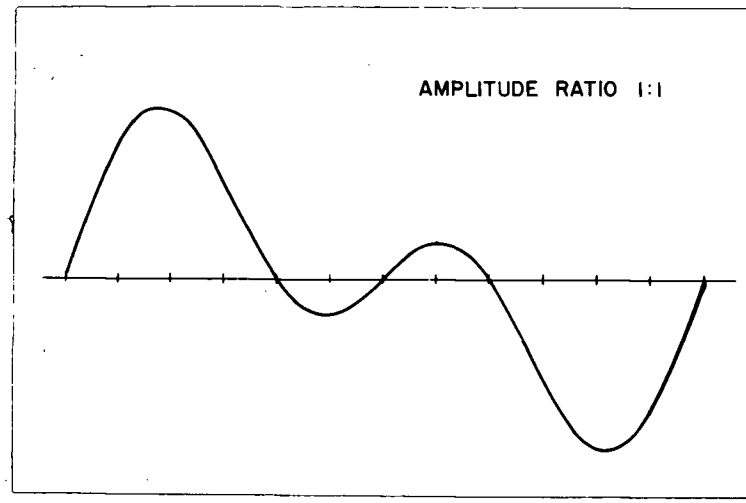

Fig. 12. Graphical Addition of Sinusoids - Frequency Ratio 2

The frequency ratio is defined as follows

$$\frac{\text{Frequency of 'Harmonic'}}{\text{Frequency of Fundamental}}$$

and the definition of the amplitude ratio is

$$\frac{\text{Amplitude of 'Harmonic'}}{\text{Amplitude of Fundamental}}$$

The important items which deserve attention in Fig. 12 are, first, the waveform involved, and, second, the relative magnitude of the two peaks involved. As the amplitude of the harmonic, twice the frequency of the

fundamental, is increased, leaving the other unchanged, the relative amplitude of the second peak increases. As long as the single frequency is finite, a relative increase of the amplitude of the second harmonic function will cause the amplitude of the second peak to approach the amplitude of the first peak. However, it will never equal it. This is an important deduction. It allows one to estimate the ratio of magnitudes involved, without carrying out a Fourier analysis.

As a final analytical derivation in this section, the RMS value of the resulting function will be determined. This is of value in the interpretation of strain frequency-spectra since, for the sake of minimization of errors, RMS values were plotted thereon.

$$V_{RMS} = \sqrt{\frac{1}{T}\int_{o}^{T} v^2 (\theta)\, d\theta}$$

To make the solution as general as possible, the following function is considered

$$V = A \sin \theta + B \sin n\theta$$

where n is an integer, $n > 1$

Substituting

$$V_{RMS} = \sqrt{\frac{1}{2}(A^2 + B^2)}$$

Consequently, the RMS value of a function consisting of the superposition of two sine functions, the frequency of one being an integral multiple of the other, in phase, is always given by the above expression.

Part 2

Different amplitude

One frequency being thrice the other

In phase

It can be shown that

$$\begin{aligned} V &= A \sin \Omega + B \sin 3\Omega \\ &= \left[A + B \left(3 \cos^2 \Omega - \sin^2 \Omega \right) \right] \sin \Omega \\ &\equiv \left[\text{Modulated amplitude} \right] (\text{circular function}) \end{aligned} \tag{18}$$

As before, the condition for a maxima, or a minima is given by

$$\cos \Omega \left[A + B \left(3 \cos^2 \Omega - 9 \sin^2 \Omega \right) \right] = 0$$

and

$$\frac{d^2V}{d\Omega^2} = - A \sin \Omega + B \sin \Omega \left(9 \sin^2 \Omega - 29 \cos^2 \Omega \right)$$

Everything said for Part 1 has a counterpart in Part 2. For similar reasons, the graphic solution of the problem, Part 2, is shown below in Fig. 13. The definition of amplitude ratio and frequency ratio is given in Part 1.

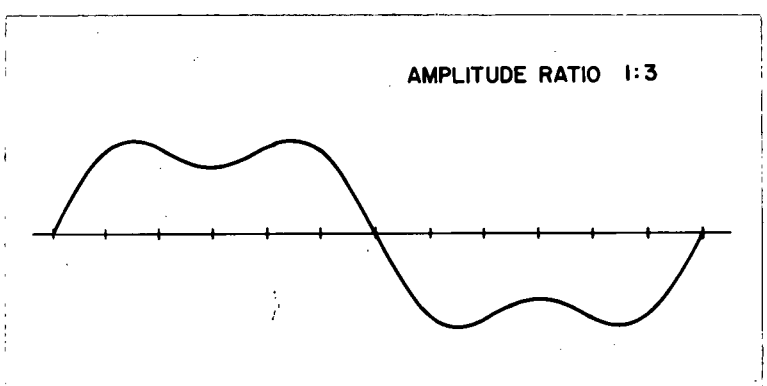

Fig. 13. Graphical Addition of Sinusoids

- Frequency Ratio 3

APPENDIX B

LINEAR EQUATIONS FOR PLATE AND BEAM

Circular Plate

The 'linear' equation of motion for transverse vibration symmetrical about the center according to $(\bar{4})$ is written

$$\left(\frac{\partial^2}{\partial r^2} + \frac{1}{r}\frac{\partial}{\partial r}\right)\left(\frac{\partial^2 W}{\partial r^2} + \frac{1}{r}\frac{\partial W}{\partial r}\right) + \frac{\varphi h}{D}\frac{\partial^2 W}{\partial t^2} = 0$$

whose solution, assuming a harmonic excitation, is

$$W(r,t) = \left[A J_o(Kr) + B Y_o(Kr) + C I_o(Kr) + \bar{D} K_o(Kr) \right] \cos \omega t$$

where

$$K^4 = \frac{\varphi h \omega^4}{D}$$

and A, B, C, and $\bar{D}$ are determined by the boundary conditions.

For a circular plate clamped in the center, with force excitation in the center and outer edge free, the natural transverse vibration is given by $(\bar{1})$ as

$$\omega_n = B_n \sqrt{\frac{Eh^2}{\varphi a^4 (1 - \nu^2)}} \quad \text{RAD/SEC}$$

and

$$B_1 = 4.35 \qquad B_2 = 24.26 \qquad B_3 = 70.39 \qquad B_4 = 138.85$$

The 'breathing mode', or the first radial vibration can be deduced from the equations listed in $(\bar{3})$

$$\frac{dJ_1 (Kr)}{d (Kr)} = J_o (Kr) - \frac{1}{Kr} J_1 (Kr)$$

By trial and error $Ka = 4.1$

but $$K = \frac{\varphi (1 - \nu^2) \omega^2}{E}$$

therefore $$f = \frac{13.94 (10)^4}{a} \quad Hz$$

Cantilever Bar

The linear equations of motion for the transverse vibration of a beam, vibrating under its own weight, assuming a harmonic excitation, is given by (9) as

$$\frac{d^4 y}{dx^4} - n^4 y = 0$$

where $$n^4 = \frac{\varphi \omega^2}{EI}$$

whose general solution is

$$y = A \cosh nx + B \sinh nx + C \cos nx + D \sin nx$$

and A, B, C, and D are determined by the boundary conditions.

The frequency equation and the respective constants according to (2) is

$$\omega_n = \frac{(r_n \ell)^2}{\ell^2} \sqrt{\frac{EI}{A\varphi}} \quad RAD/SEC$$

and $(r_1 \ell)^2 = 3.52$ $(r_2 \ell)^2 = 22.0$ $(r_3 \ell)^2 = 61.75$

$(r_4 \ell)^2 = 120.8$

The first longitudinal vibration according to (2) is calculated by using

$$\omega_n = \frac{(2n - 1)}{2\ell} \pi \sqrt{\frac{E}{\varphi}}$$

APPENDIX C

APPROXIMATE CONSTANT POWER FREQUENCY SPECTRA

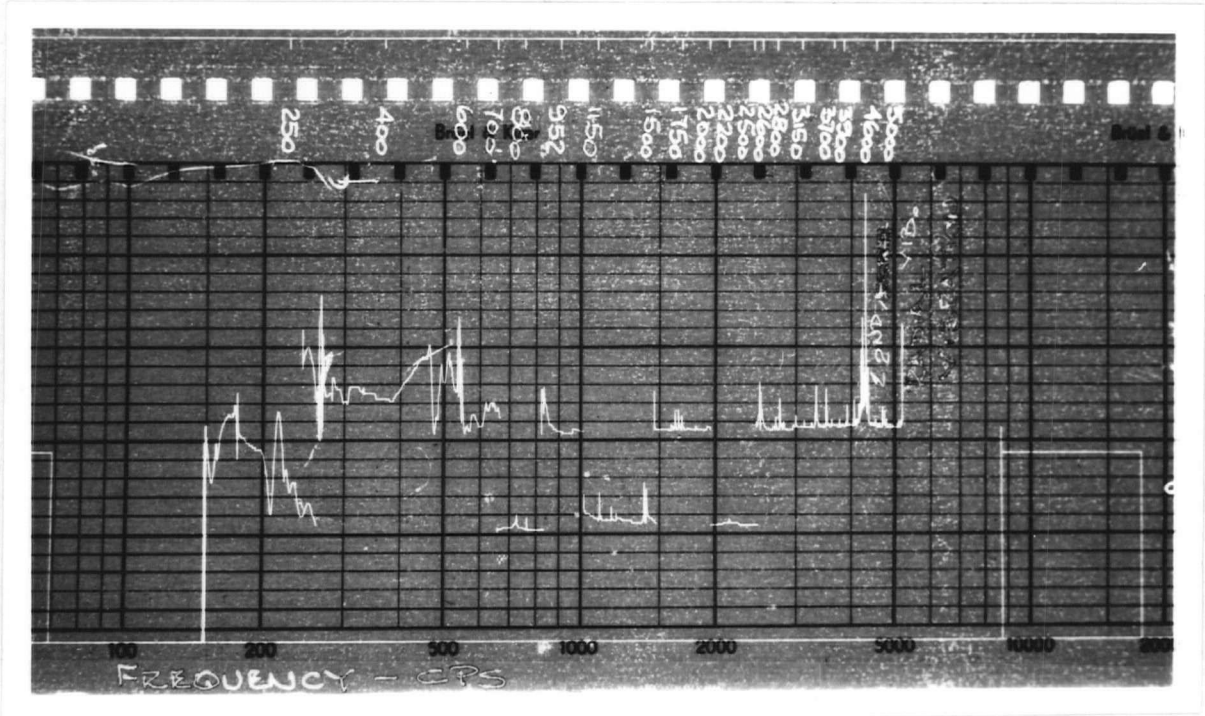

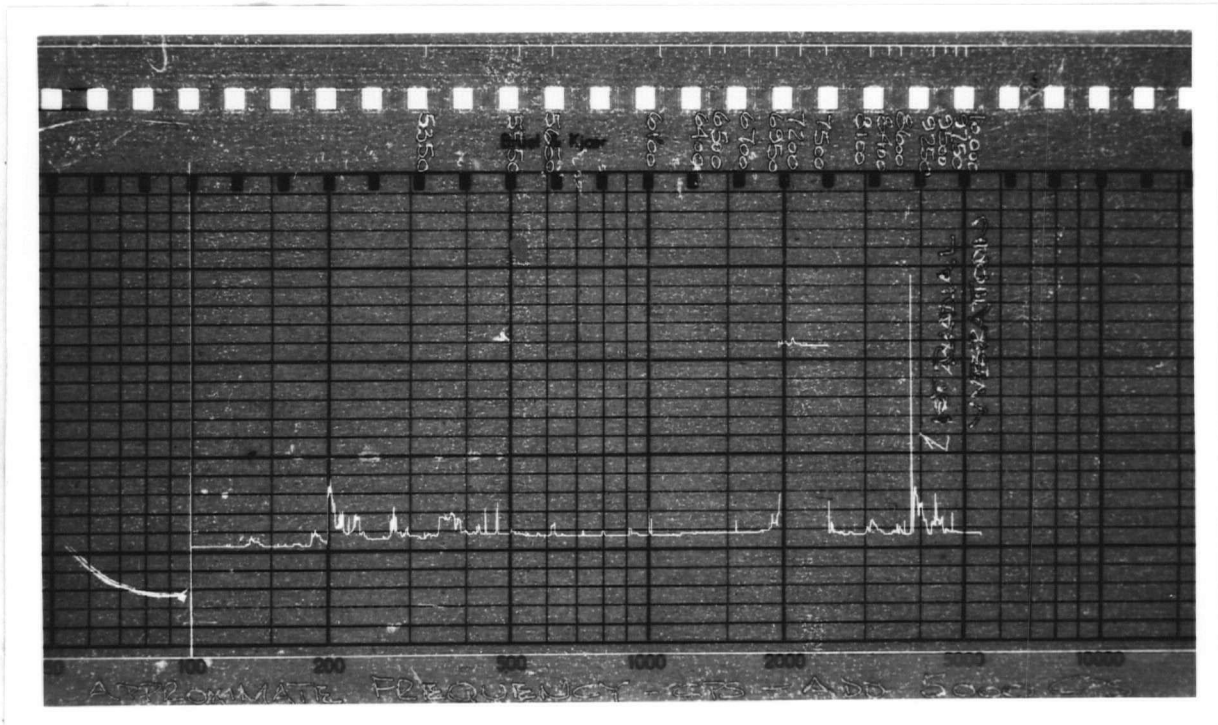

Fig. C-14. Tangential Strain Frequency Spectra for Circular Plate

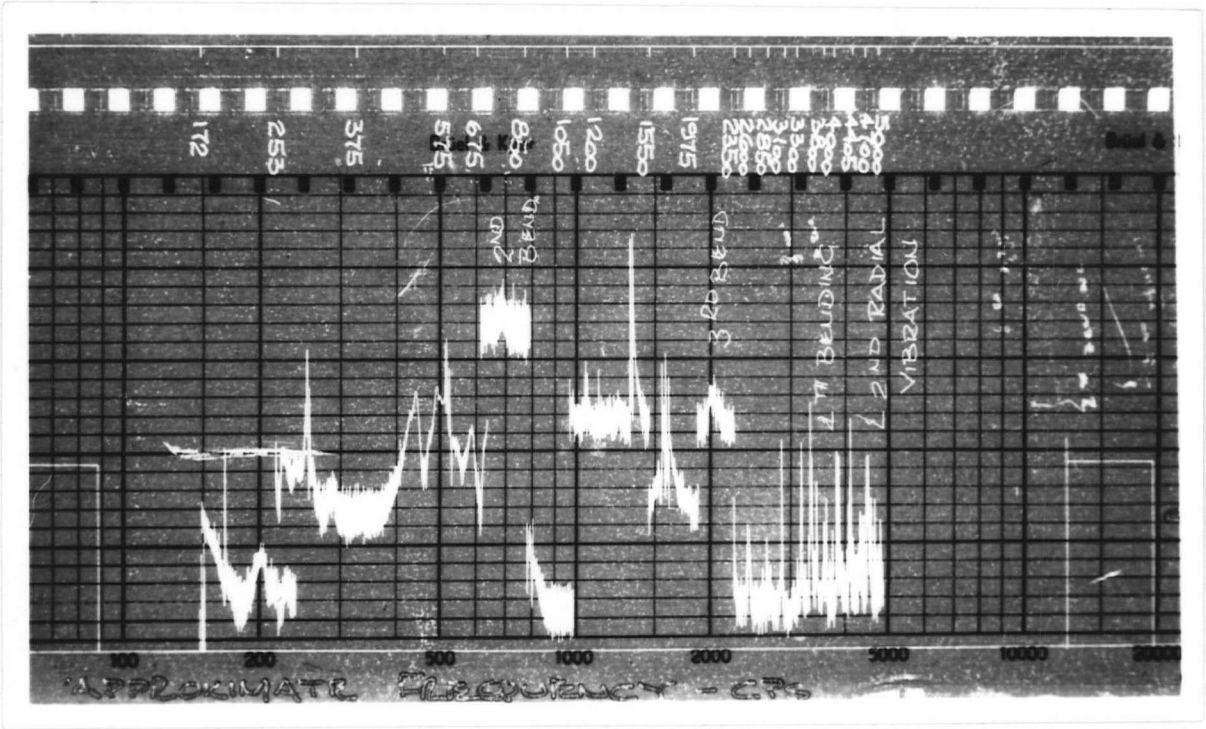

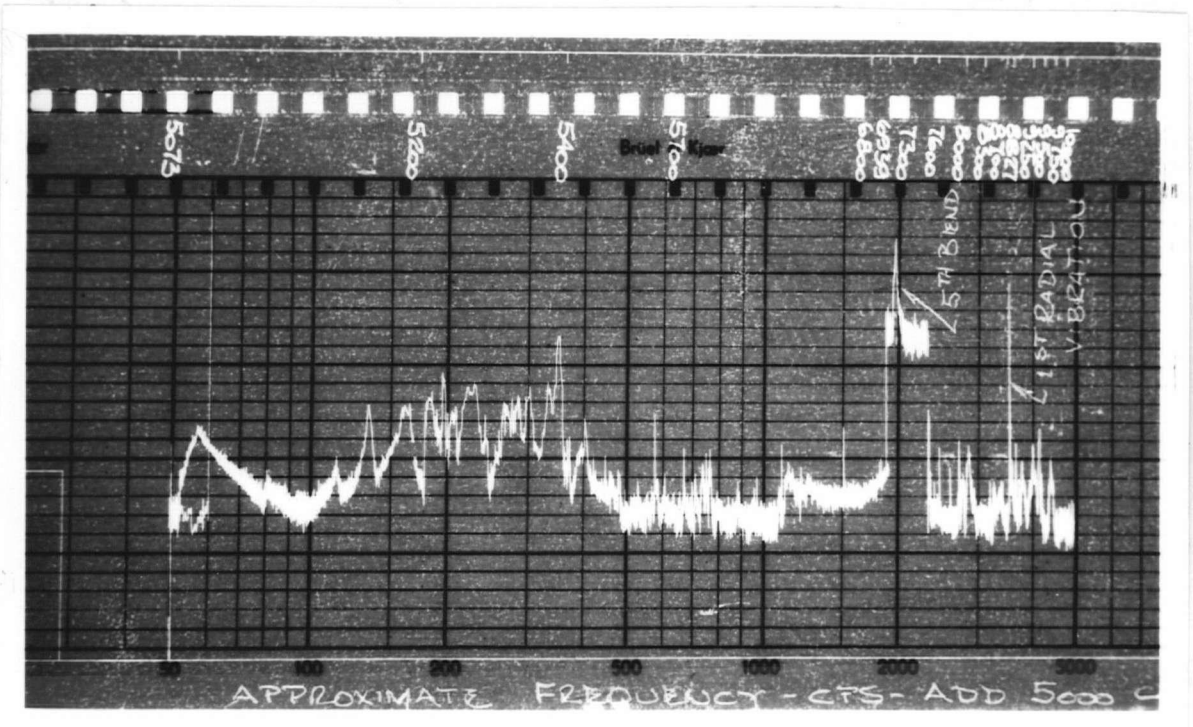

Fig. C-15. Radial Strain Frequency Spectra for Circular Plate

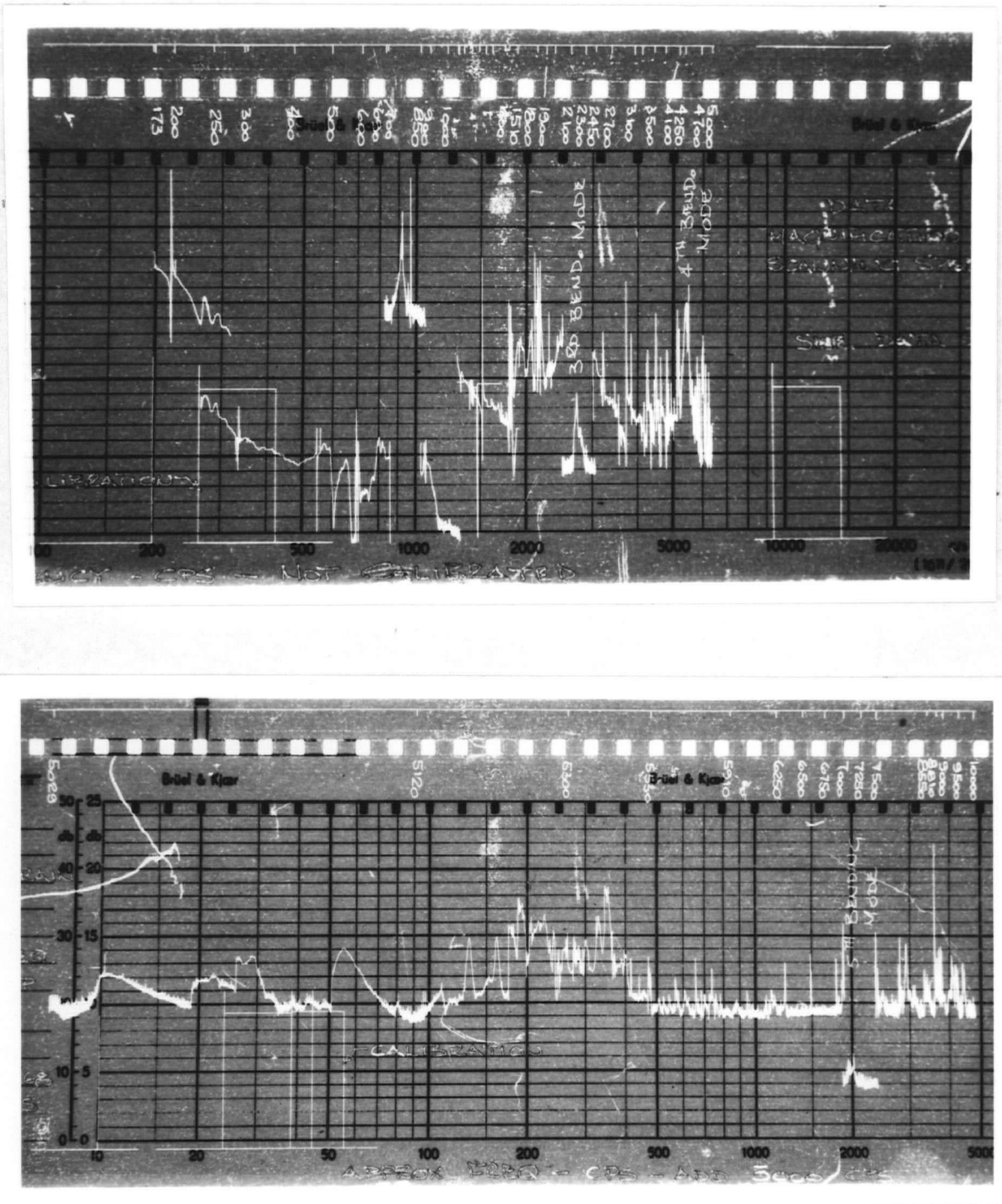

Fig. C-16. Radial plus Bending Strain Frequency Spectra for Circular Plate

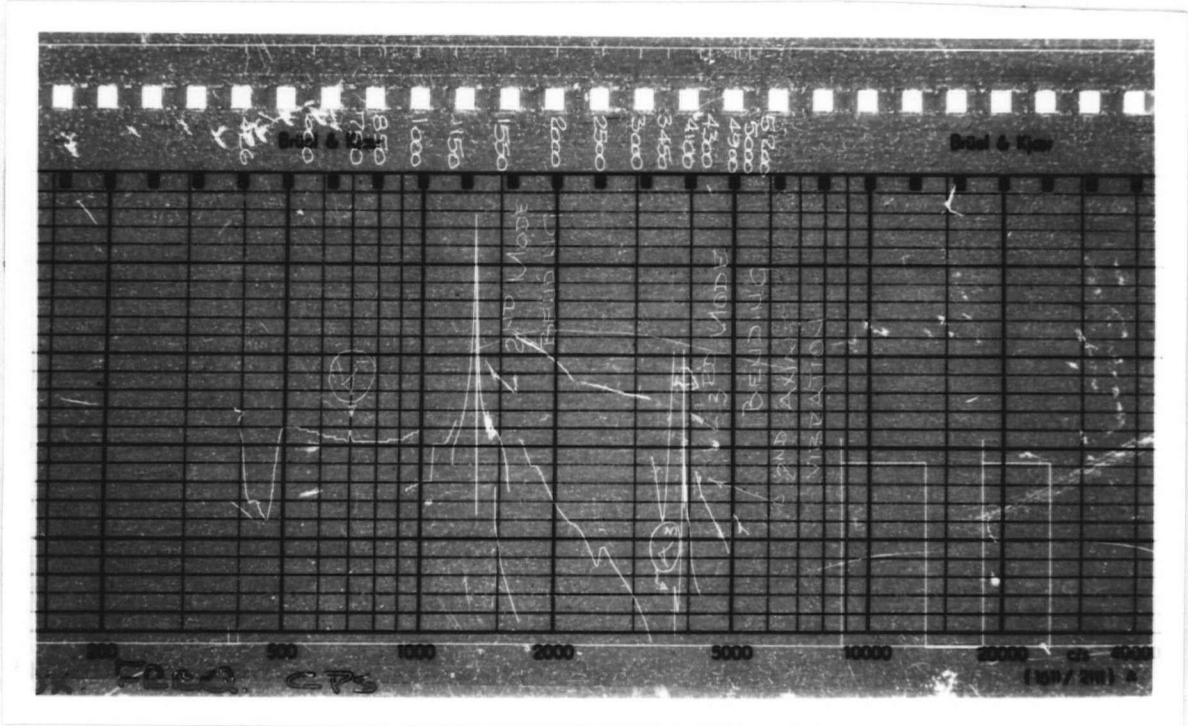

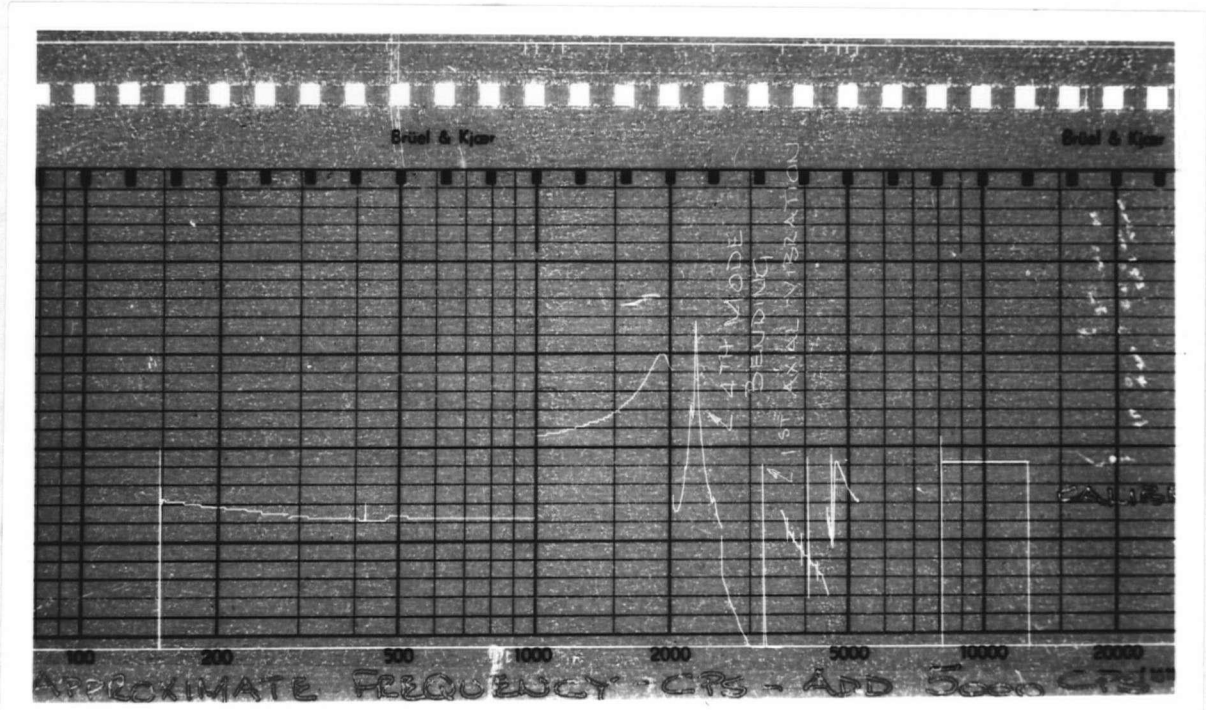

Fig. C-17. Bending plus Axial Frequency Spectra
for Cantilever Bar

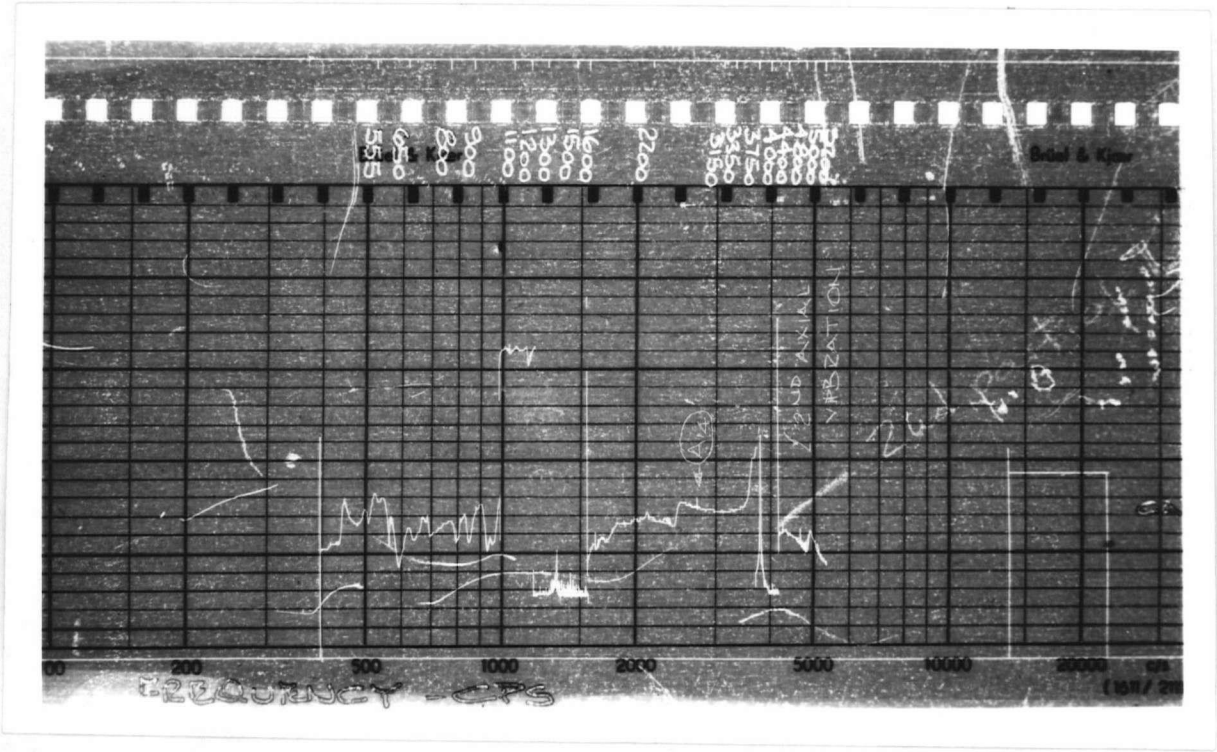

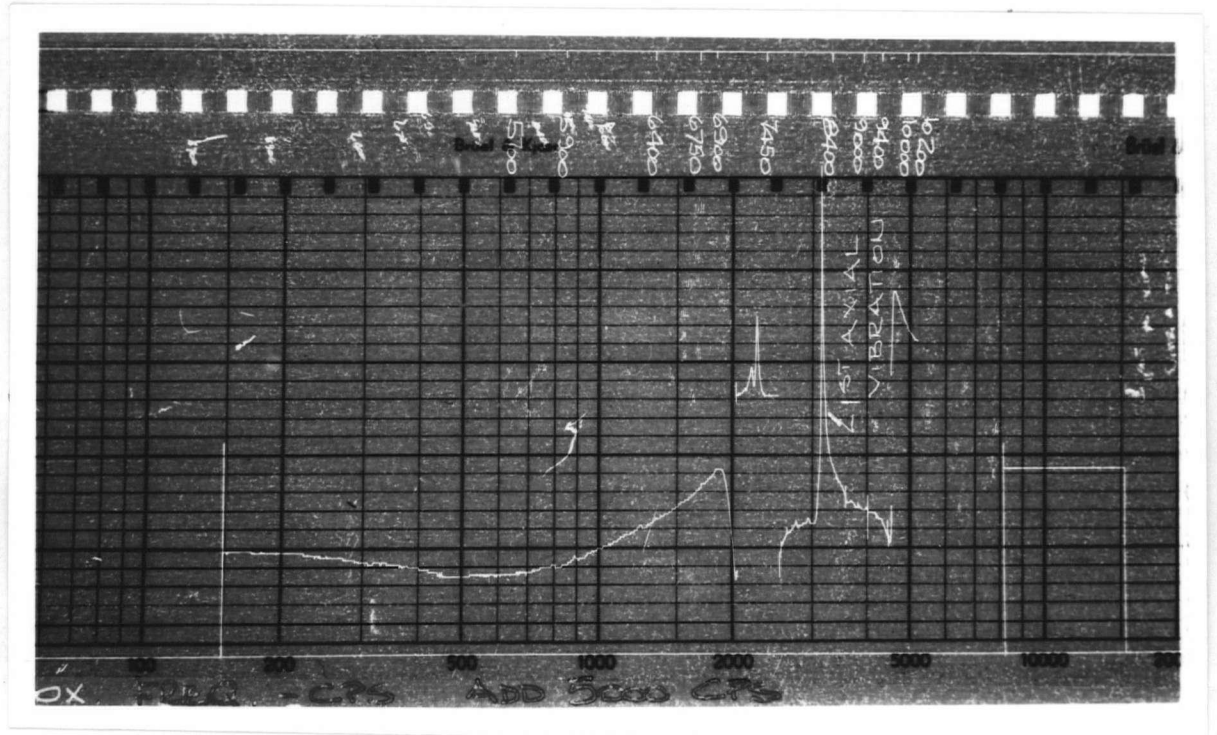

Fig. C-18. Axial Strain Frequency Spectra
for Cantilever Bar